GUT2 WP4000 Final Report

Reference: CLS-DOS-NT-11-125
Nomenclature: EUROPE
Issue: 1 rev 0
Of the: 18 May 2011

CLS 8-10 Rue Hermès - Parc Technologique du Canal - 31520 Ramonville St-Agne - FRANCE
Téléphone 05 61 39 47 00 Télécopie 05 61 75 10 14

Chronology Issues:		
Issue:	Date:	Reason for change:

People involved in this issue:		
Written by (*):	MH Rio S Mulet R. Bingham P. Knudsen O. Andersen F. Siegesmund	Date + Initials:(visa ou ref)

Distribution:		
Company	Means of distribution	Names
ESA	Electronic file	J. Benveniste S. Dinardo B. Lucas
CLS	Notification	

List of tables and figures

List of tables:

List of figures:

Applicable documents / reference documents

Pail R., Bruinsma S., Migliaccio F., Foerste C., Goiginger H., Schuh W.-D, Hoeck E, Reguzzoni M., Brockmann J.M, Abrikosov O., Veicherts M., Fecher T., Mayrhofer R., Krasbutter I., Sanso F. and Tscherning C.C. (2011): First GOCE gravity field models derived by three different approaches. *Jounal of Geodesy*, in review.

Pail R., Goiginger H., Mayrhofer R., Schuh W.-D., Brockmann J.M., Krasbutter I., Höck E., Fecher T. (2010): Global gravity field model derived from orbit and gradiometry data applying the time-wise method. *Proceedings of ESA Living Planet Symposium*, 28 June – 2 July 2010, Bergen, Norway, ESA SP-686. See also: earth.esa.int/GOCE

Migliaccio F., Reguzzoni M., Sanso F., Tscherning C.C., Veicherts M. (2010): GOCE data analysis: the space-wise approach and the first space-wise gravity field model. *Proceedings of the ESA Living Planet Symposium*, 28 June - 2 July 2010, Bergen, Norway. See also: earth.esa.int/GOCE

Bruinsma S.L., Marty J.C., Balmino G., Biancale R., Foerste C., Abrikosov O. and Neumayer H. (2010): GOCE Gravity Field Recovery by Means of the Direct Numerical Method, presented at the *ESA Living Planet Symposium*, 27th June - 2nd July 2010, Bergen, Norway; See also: earth.esa.int/GOCE

Kurtenbach, E., Mayer-Gürr T., and Eicker A. (2009), Deriving daily snapshots of the Earth's gravity field from GRACE L1B data using Kalman filtering, *Geophys. Res. Lett*., 36, L17102, doi:10.1029/2009GL039564.

Schaeffer P. et al. (2010): The new CNES CLS 2010 Mean Sea Surface, oral presentation at *OSTST 2010 meeting*; See also: http://www.aviso.oceanobs.com/en/data/products/auxiliary-products/mss/index.html

Hansen D.V., Poulain P.-M., (1996): Quality Control and Interpolations of WOCE-TOGA Drifter Data. *J. Atmos. Oceanic Technol.*, 13, 900–909.

Rio, M.-H. and Hernandez, F., (2003): High-frequency response of wind-driven currents measured by drifting buoys and altimetry over the world ocean. *Journal of Geophysical Research*, 108(C8): 3283-3301.

SSALTO/DUACS (2006), User Handbook: MSLA and MADT Near-Real Time and Delayed Products, C.L.S., Ramonville St. Agne, France.

Köhl, A., and D. Stammer, 2008, Variability of the meridional overturning in the North Atlantic from the 50 years GECCO state estimation, *J. Phys. Oceanogr., 38*, 1913–1930.

Köhl, A., D. Stammer, and B. Cornuelle, 2007, Interannual to decadal changes in the ECCO global WOCE synthesis, *J. Phys. Oceanogr., 37*, 313–337.

Marshall, J., C. Hill, L. Perelman, and A. Adcroft, 1997, Hydrostatic, quasi-hydrostatic, and nonhydrostatic ocean modelling, *J. Geophys. Res., 102*, 5733–5752.

Bingham, R., K. Haines, and C. Hughes (2008), Calculating the ocean's mean dynamic topography from a mean sea surface and a geoid, *J. Atmos. Ocean. Tech., 25*(10), 1808–1822, doi:10.1175/2008JTECHO568.1. Bingham, R., C. Tscherning, and P. Knudsen (2011),

An initial investigation of the GOCE error variancecovariance matrices in the context of the GOCE Users Toolbox project, in *Proceedings of the 4th International GOCE User Workshop, 31 March - 1 April, Munich, Germany*.

Bingham, R. J. (2010), Nonlinear anisotropic diffusive filtering applied to the ocean's mean dynamic topography, *Remote Sensing Letters*, *1*(4), 205–212, doi: 10.1080/01431161003743165.

Bruinsma, S., J. Marty, G. Balmino, R. Biancale, C. Foerste, O. Abrikosov, and H. Neumayer (2010), Goce gravity field recovery by means of the direct numerical method, in *Proceedings of the ESA Living Planet Symposium, 28 June - 2 July 2010, Bergen, Norway*, vol. (ESA SP-686, December 2010). Drinkwater, M., R. Floberghagen, R. Haagmans,

D. Muzi, and A. Popescu (2003), GOCE: ESA's first Earth Explorer core mission., *Space Science Reviews*, *108*(1–2), 419–432.

Hernandez, F., and P. Schaeffer (2001), The CLS01Mean Sea Surface: A validation with the GSFC00.1 surface, *Tech. rep.*, CLS, Ramonville St Agne, 14pp.

Jayne, S., J. Wahr, and F. Bryan (2003), Observing ocean heat content using satellite gravity and altimetry, *J. Geophys. Res.*, *108*(C2), 3031, doi: 10.1029/2002JC001619.

Koop, R., T. Gruber, and R. Rummel (2007), The status of the GOCE high-level processing facility (HPF), in *Proceedings of the 3rd GOCE User Workshop, ESRIN, Frascati*.

Migliaccio, F., M. R. amd F. Sanso, C. Tscherning, and M. Veicherts (2010), Goce data analysis: the spacewise approach and the first space-wise gravity field model., in *Proceedings of the ESA Living Planet Symposium, 28 June - 2 July 2010, Bergen, Norway*, vol. (ESA SP-686, December 2010).

Niiler, P., N. Maximenko, and J. McWilliams (2003), Dynamically balanced absolute sea level of the global ocean derived from near-surface velocity observations, *Geophys. Res. Lett.*, *30*(22), 2164, doi: 10.1029/2003GL018628.

Pail, R. e. a. (2010), Goce gravity field model derived from orbit and gradiometry data applying the time-wise method., in *Proceedings of the ESA Living Planet Symposium, Bergen, Norway*, European Space Agency.

Rhines, P., S. Hkkinen, and S. Josey (2008), Is oceanic heat transport significant in the climate system?, in *Arctic–Subarctic Ocean Fluxes*, edited by R. R. Dickson, J. Meincke, and P. Rhines, chap. 4, pp. 87–109, Springer, Netherlands.

Tapley, B., D. Chambers, S. Bettadpur, and J. Ries(2003), Large scale ocean circulation from the GRACE GGM01 geoid, *Geophys. Res. Lett.*, *30*(22), 2163, doi:10.1029/2003GL018622.

Woodgate, R., E. Fahrbach, and G. Rohardt (1999), Structure and transports of the east greenland current at 75n from moored current meters, *J. Geophys. Res.*,*104*(C8), 18,059–18,072.

Contents

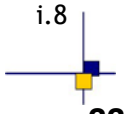

MDT	Mean Dynamic Topography
MSS	Mean Sea Surface
SLA	Sea Level Anomaly
ECCO	Estimating the Circulation and Climate of the *Ocean*
GECCO	German partner of Estimating the Circulation and Climate of the *Ocean*

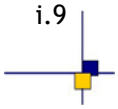

1. INTRODUCTION

The objective of this workpackage is to carry out an independent validation of the various preliminary geoid models computed by ESA HPF (High Processing Facility) from the GOCE (Gravity field and steady-state Ocean Circulation Explorer) mission in order to assess their quality for oceanographic applications.

The HPF has used three different approaches to compute the geoid models (Pail et al, 2011). The time-wise [Pail et al, 2010] and the space-wise [Migliaccio et al, 2010] approaches have been especially developed for the GOCE mission while the direct approach [Bruinsma et al, 2010] that combines orbit and gravity modelling using the orbit perturbation theory, is more classical. Two releases computed from respectively 2 months and 6 months of GOCE data are available for each geoid model based on the time-wise and the direct approaches. Only one release based on the space-wise approach is available and uses 2 months of GOCE data.

The two releases based on the direct approach (EGM_DIR_R1 and EGM_DIR_R2) are developed to order and degree 240 of spherical harmonics (83 km resolution). EGM_DIR_R1 results from 2 months of GOCE data constrained toward Eigen_51C that combines surface and GRACE data [Bruinsma et al, 2010] while EGM_DIR_R2 results from 6 months of GOCE data constrained toward ITG_Grace2010s that is a GRACE (Gravity Recovery And Climate Experiment) only solution. The first release based on the time-wise approach (EGM_TIM_R1) is developed to order and degree 224 of spherical harmonics (89 km resolution) while the second release (EGM_TIM_R2) is developed to order and degree 250 (80 km resolution). EGM_SPW is based on the space-wise approach and is developed to order and degree 210 of spherical harmonics (95 km resolution).

In order to evaluate the accuracy of the different GOCE geoid models described above for oceanographic use, they were used to determine the ocean MDT (Mean Dynamic Topography). The ocean Mean Dynamic Topography is the simple difference between an altimetric Mean Sea Surface (MSS – Mean sea level above a reference ellipsoid) and a geoid model (relative to the same ereference ellipsoid). A MSS resolves spatial scales as short as 10-20 km while the geoid models are developed up to degree and order 210-250 (i.e. 95-80 km resolution). Further filtering is hence needed. In the following sections, different filtering methods are used: Classical Gaussian filters are used in sections 2, 3 and 5 while an anisotropic diffusive filter is applied in section 4

The various MDT obtained were subsequently compared with other MDT estimates derived using other geoid models (based on GRACE data), or computed from the use of in-situ oceanographic data (sections 2, 3 and 4) or ocean general circulation models (section 5). The MDT comparisons were carried out by analysing MDT residuals as well as their associated geostrophic surface currents at different maximum harmonic. Both the impact of the different methodolgies used to compute the gravity field as well as the contribution of the four months of supplementary data have been checked. Finally, both global (sections 2 and 5) and regional (sections 3 and 4) assessments have been performed.

2. COMPARISON OF GOCE MDTs TO DRIFTING BUOY VELOCITIES

2.1. METHOD

In order to investigate the quality of the new GOCE geoid models we have first compute MDTs from EGM_DIR, EGM_SPW and EGM_TIM. To quantify the improvement of GOCE relative to GRACE mission we have also computed a MDT from ITG-Grace2010s developed to order and degree 180 and using seven years of GRACE data [Kurtenbach et al, 2009].

The MDTs are computed by subtracting the different geoid models from an altimetric Mean Sea Surface. The Mean Sea Surface used in this section is the MSS_CNES_CLS10 estimated for the 1993-1999 period [Schaeffer et al, 2010]. The MSS resolves spatial scales as short as 10-20 km while the geoid models are developed up to degree and order 210-250 (i.e. 95-80 km resolution) for the GOCE solutions and up to degree and order 180 (i.e. 111 km resolution) for the GRACE solution. Further filtering is hence needed. We applied a gaussian filter using for the resolution scales six different values (100, 125, 150, 200, 250 and 350 km).

We have mainly focused on the geostrophic currents deduced from the MDTs that are an estimation of the MDT gradients and thus are more sensible to noise than the MDT itself. Moreover it is more convenient to have a reliable estimate of geostrophic currents from in-situ data than an estimate of height above geoid. The estimate of the mean geostrophic currents (called 'synthetic' currents in the following) is deduced from all the 15 meter drogued drifting buoy data collected from 1993 to 2008 in the framework of the international WOCE and TOGA Surface Velocity Program (Figure 1). These data are distributed by AOML where they first have been quality controlled and krigged [Hansen and Poulain, 1996] in order to provide 6-hourly velocity measurements. In order to extract from the drifting buoy velocities only the geostrophic component, the Ekman current was first modelled [Rio et al, 2010] and subtracted. Then, a 3 day low pass filter was applied to the velocities to remove inertial and tidal currents as well as residual high frequency ageostrophic currents. Finally the geostrophic velocity anomalies deduced from the Sea Level Anomalies relative to the 1993-1999 period are interpolated along the drifter's trajectories and substracted from the associated instantaneous geostrophic currents to have an estimate of the mean geostrophic currents relative to the same 7 year period. The altimetric SLAs used in this study are computed by the SSALTO/DUACS center and distributed by AVISO [SSALTO/DUACS, 2006]. The synthetic currents obtained as described above are then filtered at the same resolution scales and using the same gaussian filter than the MDTs computed from geoid models.

Standard deviations of the differences between the geostrophic currents associated with MDTs computed from geoid models and synthetic geostrophic currents deduced from independent observations are computed at different resolution scales. The results will be discussed in the following sections.

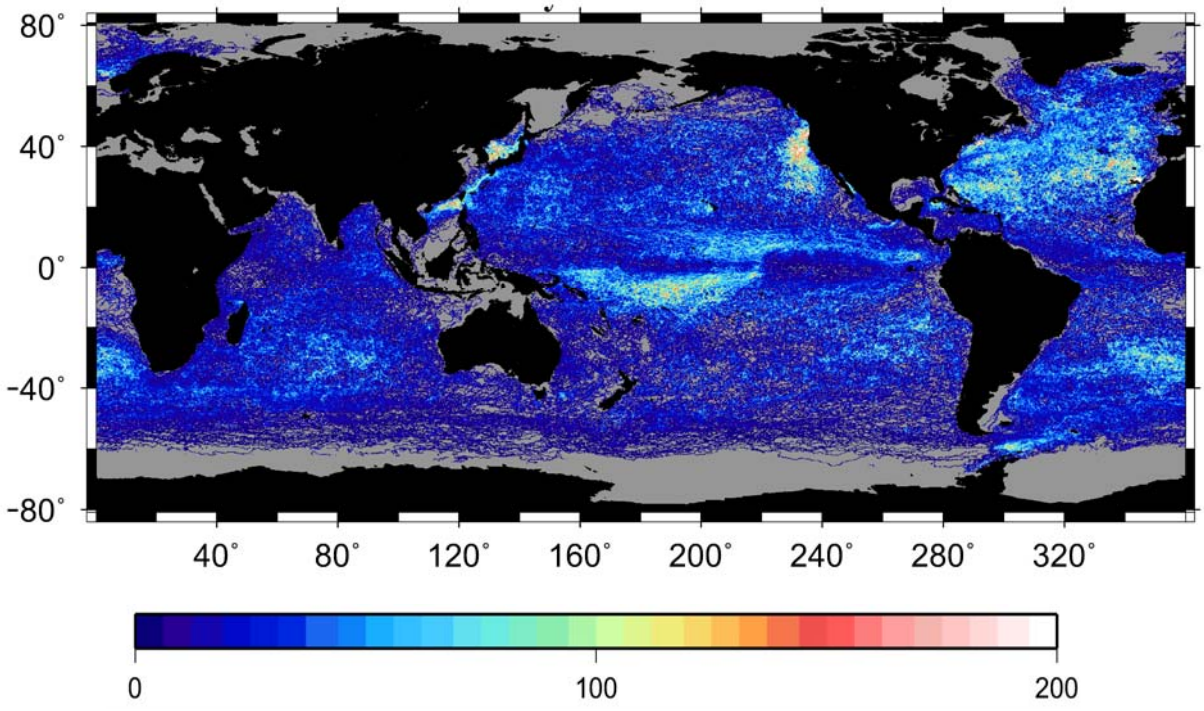

Figure 1: Number of drifting buoy velocities available for the period 1993-2008 in ¼° boxes.

2.2. Impact of the MSS in the computation of direct MDT

In Figure 2 we show the RMS differences between unfiltered synthetic velocities and geostrophic velocities derived from MDTs computed using the EGM_DIR_R1 geoid model but different altimetric MSS (CLS01, CNES-CLS10, DNSC08 and DTU10). The GOCE MDTs have been filtered at different spatial scales ranging between 50 and 500 km.

We chose to use the CNES_CLS10 MSS and we will compare it with the MDT_CNES_CLS09 that have been computed on the same period (1993-1999). Slightly better results (reduced RMS differences for both the zonal and the meridian components of the velocities) are obtained using the CNES-CLS10 MSS for scales ranging between 100 and 250km. This may be partly due to the fact that the altimetric corrections applied for the generation of the AVISO SLA used to compute the synthetic mean velocities are more consistent with the CNES-CLS10 solutions than with the DNSC and DTU solutions. This highlights the importance of using consistent altimetric datasets (MSS, MDT, SLA) when computing the ocean absolute dynamic topography (and the derived ocean geostrophic currents). In the following we will therefore use the CNES-CLS10 MSS.

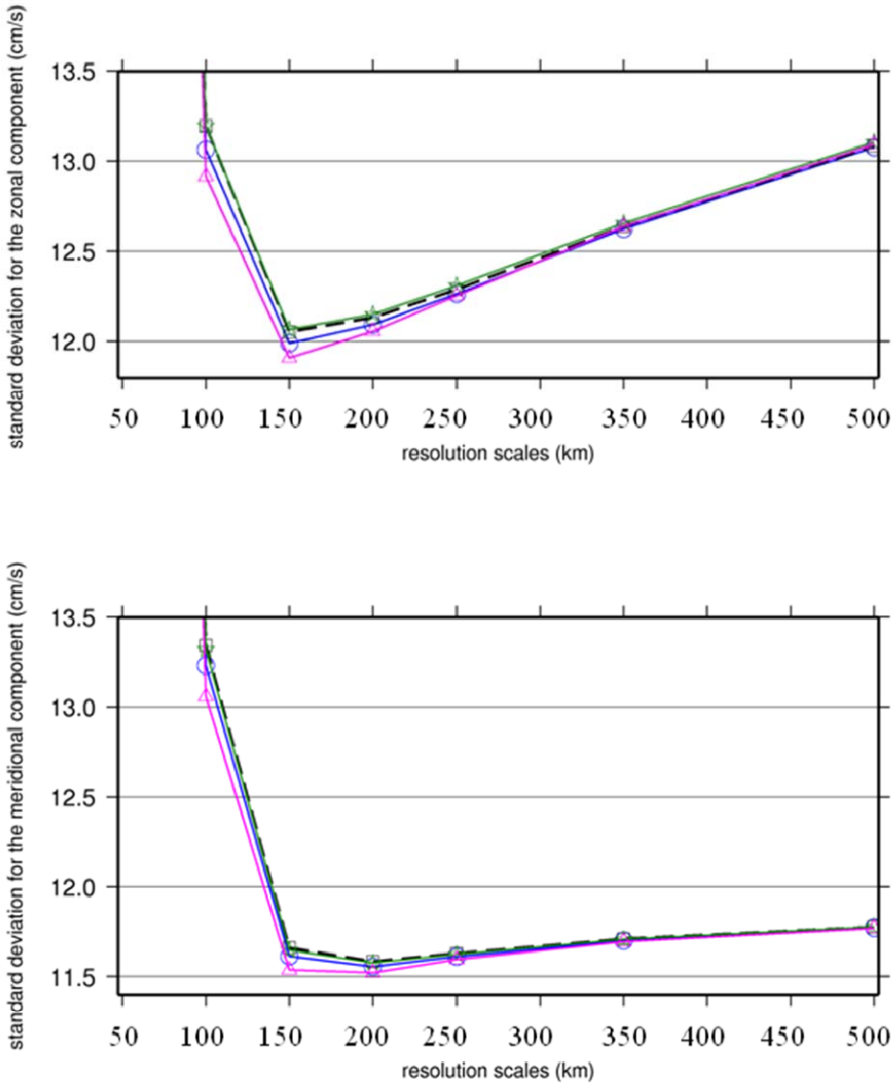

Figure 2: Standard deviation of the differences between the unfiltered synthetic geostrophic velocity components (zonal on top and meridional at the bottom) and the filtered geostrophic velocity components from different 'direct' MDT estimates obtained from the same geoid model (EGM_DIR_R1) but different MSS: (black squares) DNSC08, (green stars) DTU10, (blue circle) CNES_CLS01 and (pink triangle) CNES_CLS10.

2.3. IMPROVEMENT OF GOCE OVER GRACE

Figure 3 shows, at different resolution scales, the standard deviation of the differences between synthetic geostrophic currents and geostrophic velocities estimated from GRACE and GOCE MDTs. In this part, only the first release of the GOCE geoid models computed with 2 months of data are used.

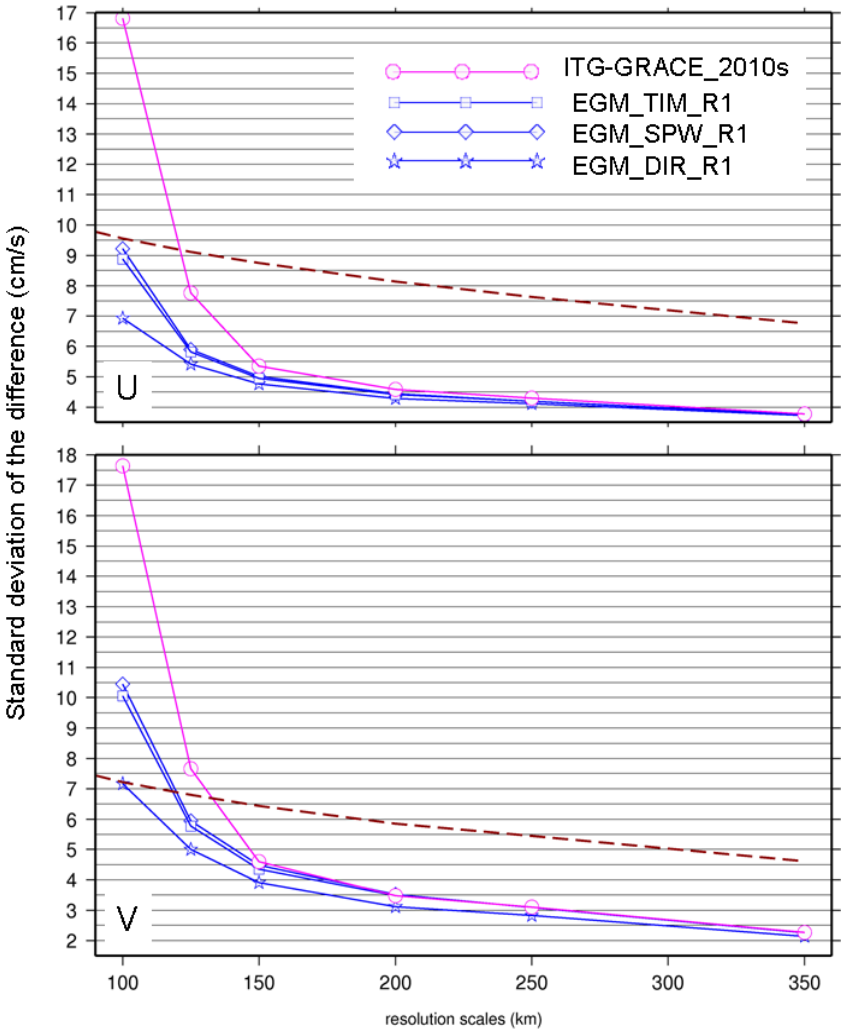

Figure 3: Standard deviation over the global ocean of the difference between the synthetic geostrophic currents and geostrophic currents associated with MDTs computed from (pink circles) ITG_GRACE2010s, (blue squares) EGM_TIM_R1, (blue diamonds) EGM_SPW_R1 and (blue stars) EGM_DIR_R1 .The top plot (resp. bottom) shows results for the zonal (resp. meridional) component. The red dash line shows the standard deviation of the synthetic estimate of the mean geostrophic velocities.

At scales smaller than 200 km, the standard deviations of the differences are much smaller with MDTs computed with GOCE geoid models (blue lines) than with GRACE geoid model (pink lines). At 100km, GOCE improves a lot the comparisons to independent observations; the gain of EGM_TIM_R1 compared with

ITG_Grace2010s $\left(\frac{\sigma^2_{ITG-Grace2010s} - \sigma^2_{EGM\_TIM}}{\sigma^2_{ITG-Grace2010s}} \right)$ is 72% for the zonal velocities and 68% for the meridional velocities. In the Gulf Stream area (Figure 4) the circulation is well described by MDTs computed with GOCE data while MDT computed with ITG_Grace2010s is very noisy. At 150 km GOCE geoid models give standard deviations of the differences (Figure 3) smaller by more than 1.5cm/s than ITG_Grace2010s and smaller than the synthetic variability itself (red dash lines) for both components. At these scales, only 2 months of GOCE data improve a lot the mean oceanic circulation compared with 7 years of GRACE data.

At scales larger than 200-300km, the difference between geoid heights estimated from GRACE data and GOCE data are less than 1.5 cm. Thus, it is difficult to see this difference studying MDTs. At these scales GOCE and GRACE have similar performances for the computation of Mean Dynamic Topography.

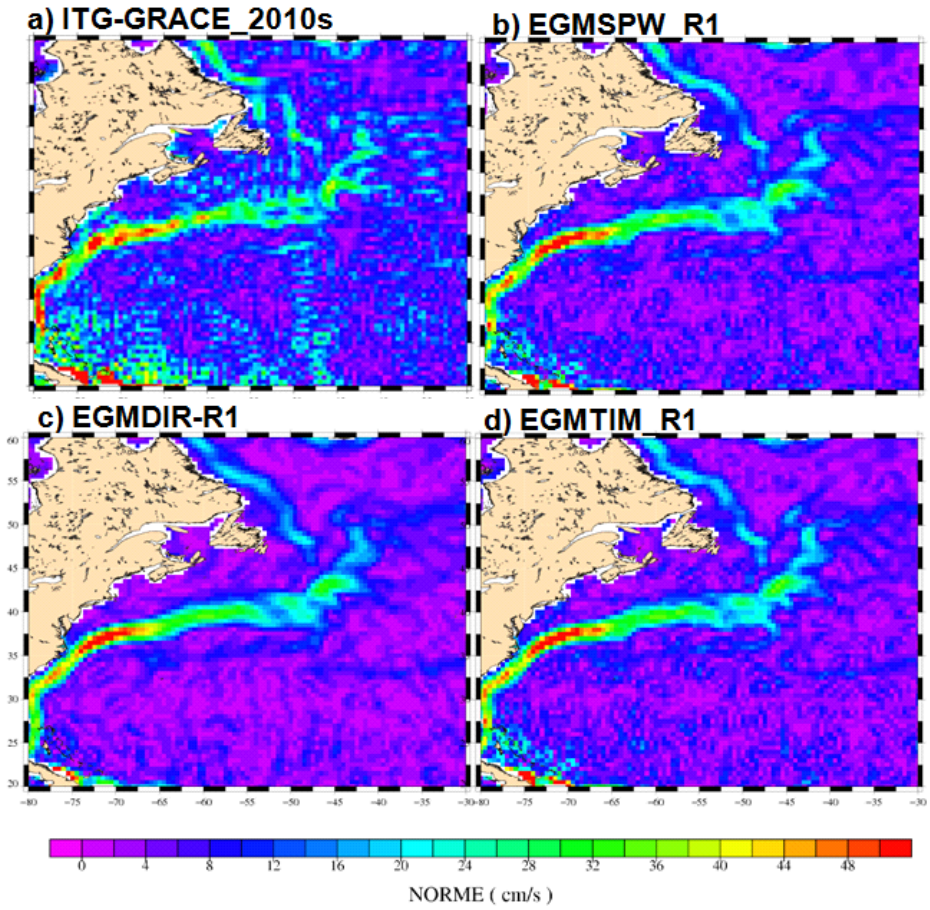

Figure 4: Intensity of the mean geostrophic currents (cm/s) in the Gulf Stream area from the 100km-filtered MDTs computed from (a) ITG-GRACE2010s, (b) EGM_SPW_R1, (c) EGM_DIR_R1 and (c) EGM_TIM_R1

2.4. COMPARISON BETWEEN THE DIFFERENT APPROACHES

In this section, we investigate the impact of the different approaches (time-wise, space-wise and the direct one) used to compute the GOCE geoid models in the final estimation of the mean oceanic circulation.

The blue lines on Figure 3 show the results of the comparison to independent observations for the different approaches used in the first HPF release. EGM_DIR_R1 is constrained toward Eigen51C, a geoid model that combines GRACE and surface data. The surface data help to improve small scales compared with the satellite only geoid models. Thus, it is not surprising that the direct approach gives smaller standard deviations of the difference than the other approaches. EGM_SPW_R1 and EGM_TIM_R1 give almost similar results, the space-wise approach give slightly smaller standard deviations.

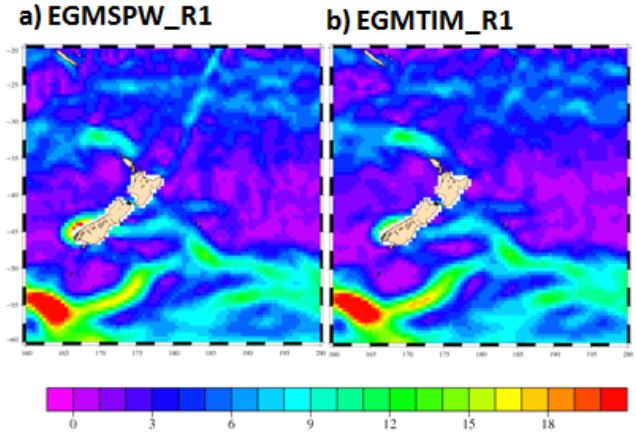

Figure 5: Intensity of the mean geostrophic currents (cm/s) in the New Zealand area from the 150km-filtered MDTs computed from (a) EGM_SPW_R1 and (b) EGM_TIM_R1.

Figure 5 illustrates that the space-wise approach is a bit noisier than the time-wise approach in the North-East of New Zealand. In this area, the high gravity gradients on the boundary between the Pacific and the Indo-Australian Plates are hardly resolved in the geoid models. On the contrary the Mean Sea Surface has higher resolution and resolves these kinds of structures. As a result, unrealistic circulation patterns are found in the MDT computed by subtracting the MSS and the geoid height.

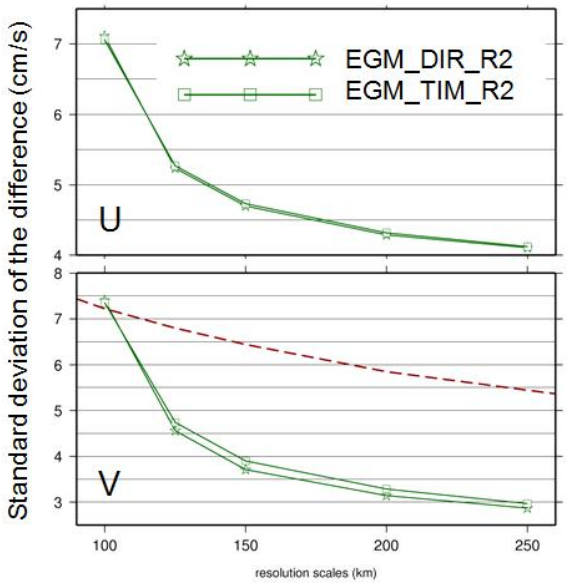

Figure 6: Standard deviation over the global ocean of the differences between the synthetic geostrophic currents and geostrophic currents associated with MDTs computed from (green squares) EGM_TIM_R2 and (green stars) EGM_DIR_R2 .The top plot (resp. bottom) shows results for the zonal (resp. meridional) component. The red dash line shows the standard deviation of the synthetic estimate of the mean geostrophic velocities.

On Figure 6, we compare the geoid models from the second HPF release. EGM_DIR_R2 and EGM_TIM_R2 give globally similar results. Differences are seen depending on the area. South of Australia (Figure 7) where the computation of the geoid models is difficult because of the influence of the magnetic pole, the MDT computed with EGM_DIR_R2 is more noisy than the one computed with EGM_TIM_R2. However, it is the contrary In the Kuroshio area (Figure 8a and Figure 8c).

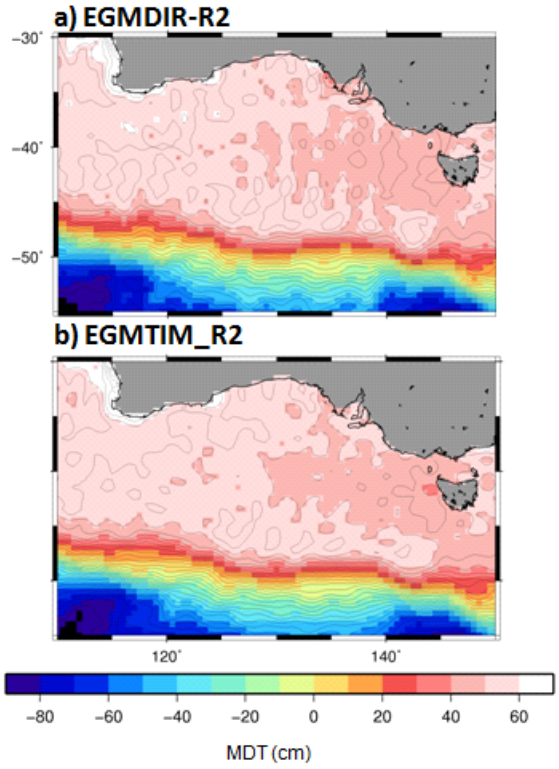

Figure 7: Mean Dynamic Topography (cm) filtered at 100 km south of Australia computed from (a) EGM_DIR_R2 and (b) EGM_TIM_R2.

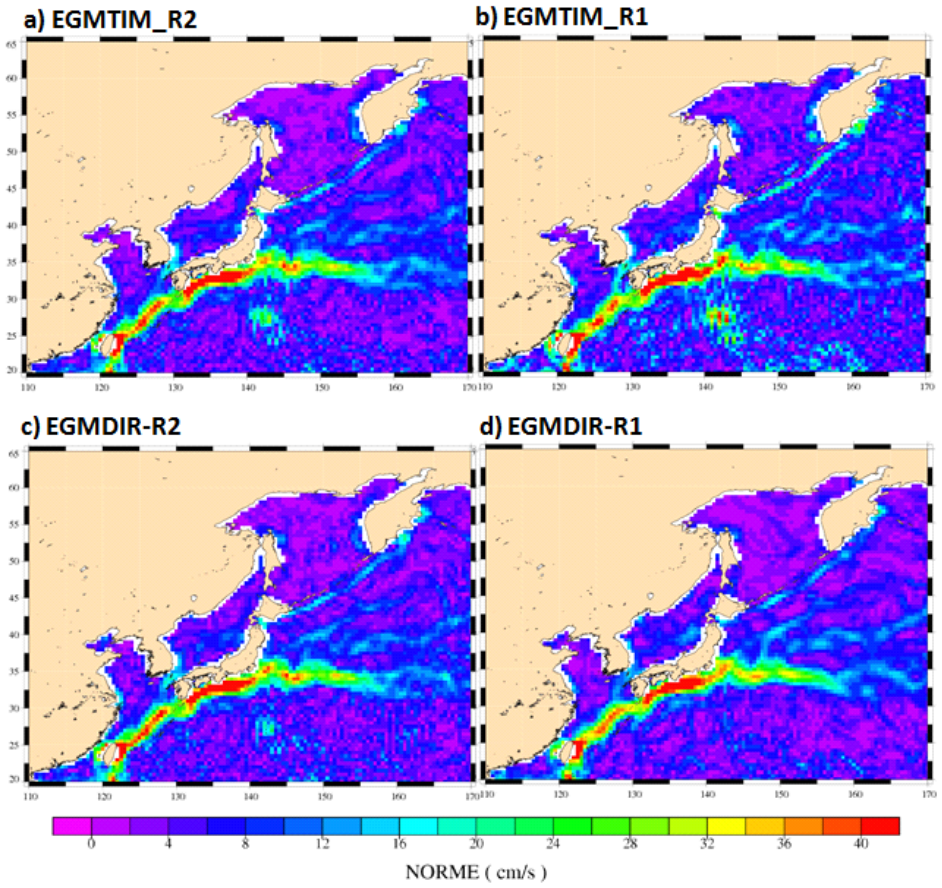

Figure 8: Intensity of the mean geostrophic currents (cm/s) in the Kuroshio area from the 100km-filtered MDTs computed from (a) EGM_TIM_R2, (b) EGM_TIM_R1, (c) EGM_DIR_R2 and (d) EGM_DIR_R1.

2.5. IMPACT OF MORE GOCE DATA

In this part we will compare the first HPF release computed with 2 months of GOCE data and the second HPF release computed with 3 times more GOCE data.

First, the comparison between the first and the second releases of EGM_TIM permits to quantify the impact of using more GOCE data in a GOCE only geoid model.

Figure 9 shows that using 3 times more GOCE data improves a lot the comparison to independent observations. At 100km, the standard deviation of the differences for the zonal (resp. meridional) velocities decreases by about 2 cm/s (resp. 2.5 cm/s) with EGM_TIM_R2 compared with EGM_TIM_R1, the gain is 36 % (resp. 46 %). Figure 10 and 12 illustrate the improvement. The MDT computed with the second release of EGM_TIM is globally less noisy than the first release (Figure 10); the improvement is especially visible in the interior and east of the subtropical gyres and south of Australia. Figure *8*a and Figure *8*c show the improvement in the Kuroshio area.

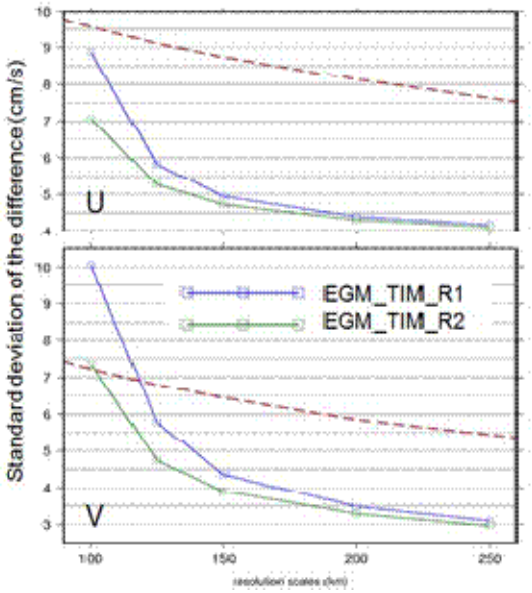

Figure 9: Standard deviation over the global ocean of the difference between the synthetic currents and currents associated with MDTs computed from (blue squares) EGM_TIM_R1 and (green squares) EGM_TIM_R2. The red dash line shows the standard deviation of the synthetic currents.

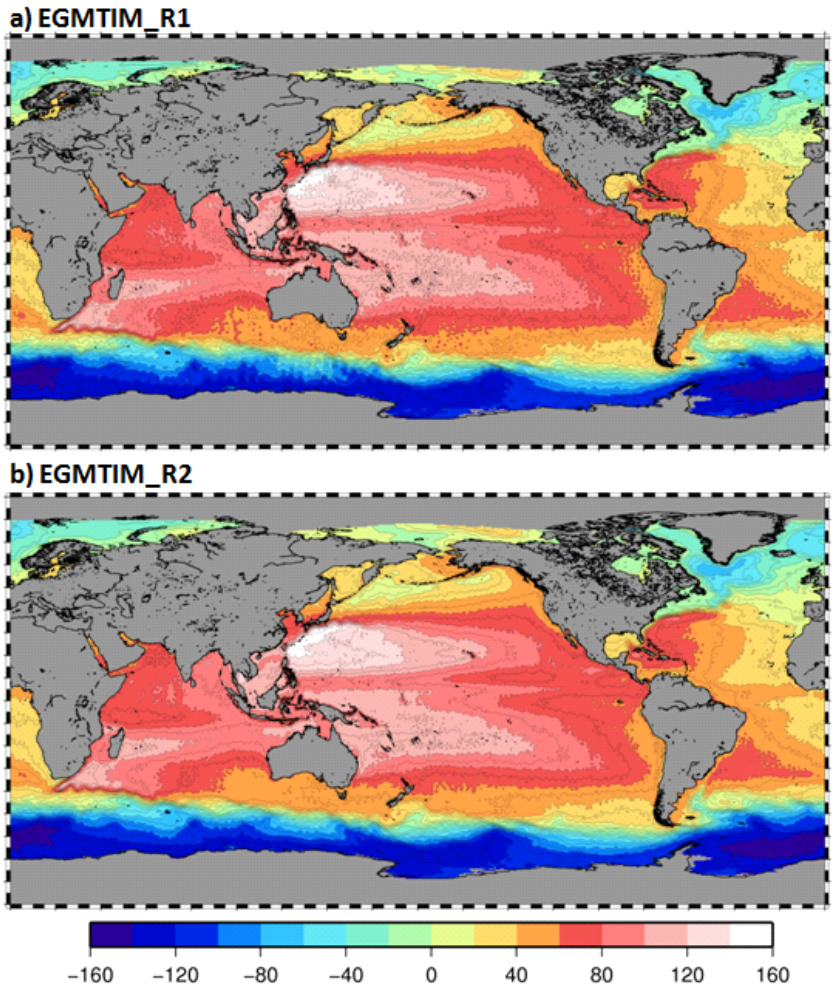

Figure 10: Mean Dynamic Topography (cm) filtered at 100 km and computed from (a) EGM_TIM_R1 and (b) EGM_TIM_R2.

Then, Figure 11 shows the results of the comparison to independent observations for the different geoid models using the direct approach. EGM_DIR_R1 and R2 are both constrained toward an apriori geoid model but not the same. As already mentioned earlier, EGM_DIR_R1 is constrained toward Eigen_51C that combines surface and GRACE data while EGM_DIR_R2 is constrained toward ITG_Grace2010s (GRACE only solution). To quantify the impact of more GOCE data, we compare EGM_DIR_R1 (blue stars on Figure 11) and a model computed using exactly the same approach but with more GOCE data (yellow stars on Figure 11). The improvement is less significant than for the time-wise approach (about 1cm at 100 km) because the surface data including in Eigen_51C already give information about small scales. However, this comparison brings a significant information regarding the significant contribution of GOCE data for improving geoid models that include surface data. At 100km, EGM_DIR_R1 gives better results than EGM_DIR_R2 thanks to the surface data. Figure *8*c and Figure *8*d illustrate that EGM_DIR_R2 is noisier than EGM_DIR_R1 in the Kuroshio area at 100 km resolution scale. But between 120 and 200 km, EGM_DIR_R2 behaves slightly better (Figure 11). Thus, the use of 4 supplementary months of GOCE data improves mostly scales between 120 and 200 km compared with a model that combines surface and GRACE data.

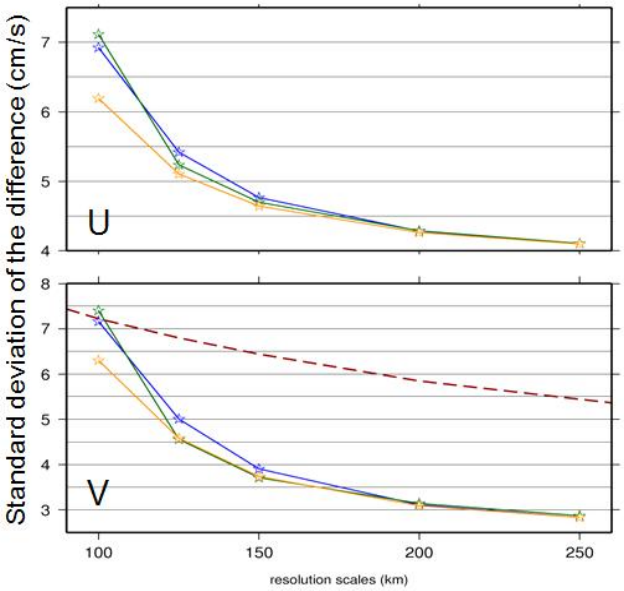

Figure 11: Standard deviation over the global ocean of the difference between the synthetic estimate of mean geostrophic velocities and geostrophic currents associated with MDTs computed from (blue stars) EGM_DIR_R1, (green stars) EGM_DIR_R2 and (yellow stars) a geoid model equivalent to EGM_DIR_R1 but with 6 months of GOCE data. The top plot (resp. bottom) shows results for the zonal (resp. meridional) component. The red dash line shows the standard deviation of the synthetic estimate of the mean geostrophic velocities.

2.6. CONCLUSIONS

The computation of Mean Dynamic Topographies from different geoid models and the comparisons with independent data from in-situ oceanographic measurements and altimetry has permitted to carry out an independent validation of the preliminary GOCE Level-2 products at different resolution scales. Only 2 months of GOCE data improve a lot the scales smaller than 200 km (DO 100) compared with ITG-Grace2010s, a geoid model computed with seven years of GRACE

data. Using three times more GOCE data improve a lot the GOCE only geoid models but the improvement is less significant when using a geoid model that combines surface and satellite data. In a combined geoid model, GOCE improves mostly scales between 120 km (DO 166) and 200 km (DO 100).

3. Regional zoom n°1: Assessment of GOCE MDT accuracy in the Mediterranean Sea

The Mediterranean Sea is a challenging region for the use of GOCE data in oceanography, since the spatial scales of the oceanic structures are smaller than in the open ocean and, in many places, smaller than the expected resolution of GOCE (100km). In this section, we have investigated if the preliminary GOCE geoids are accurate enough to be useful for retrieving the Mediterranean Sea mean circulation. The bottom of Figure 12 shows the MDT computed from the CNES-CLS10 MSS and the EGM-DIR2 geoid model at 150km (left) and 200km (right) resolution. Compared to what was obtained with the last GRACE geoid model (ITG-GRACE2010s, top), the use of GOCE data allows to retrieve a less noisy MDT.

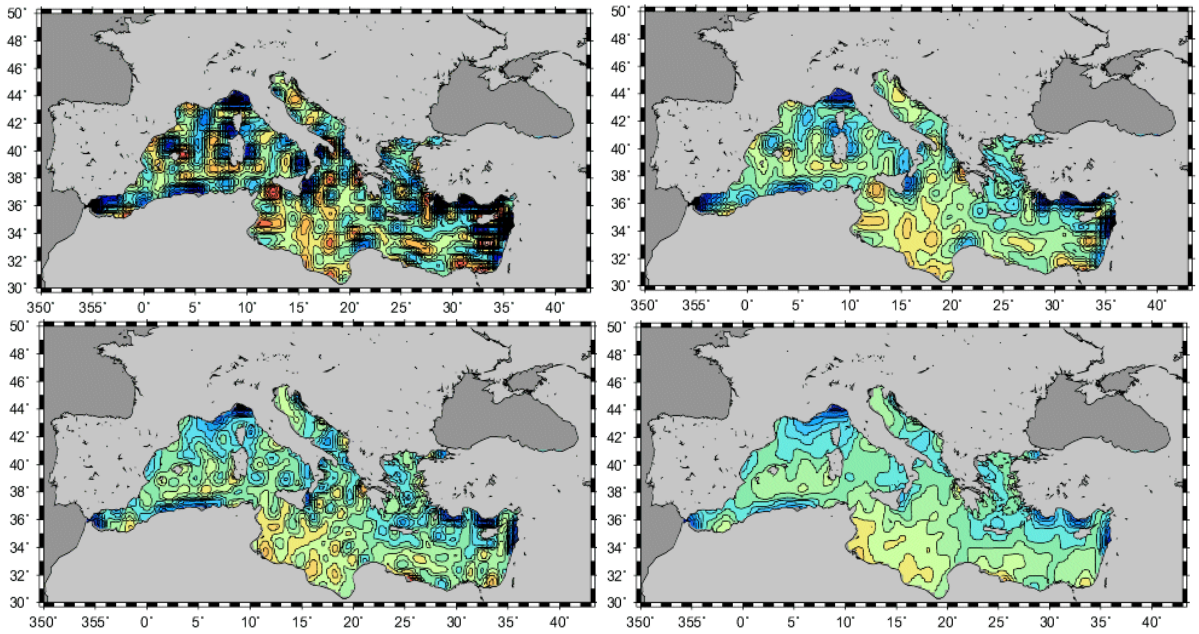

Figure 12: MDT in the Mediterranean Sea computed from the CNES-CLS10 MSS and (top) the ITG-GRACE2010S (bottom) the EGM-DIR2 geoid model. Left column: A 150km low pass filter is applied Right column: A 200km low-pass filter is applied

For comparison, the Figure 13 shows the MDT computed in the Mediterranean Sea by Rio et al, 2007 from a combination of model outputs, drifter velocities and altimetric data. Consistent patterns are obtained in the center of the Ionian Sea (the Ionian jet is resolved by the GOCE MDT at 200km resolution), and in the North Western basin, where a low is visible both in the SMDT07 and the GOCE MDT. Elsewhere, however, it is difficult to distinguish the main circulation patterns of the Mediterranean Sea in the GOCE MDT. Along the North African coast, the Algerian current is directed westward in the GOCE MDT, whereas it is a well-known eastward flowing current, very well depicted by the use of drifting buoy velocities as shown on Figure 14. In this specific case of a very narrow, intense, coastal jet, the resulting MDT might well be polluted by strong errors on the altimetric Mean Sea Surface. This issue is important to take into account is the best exploitation of GOCE data has to be made in this area.

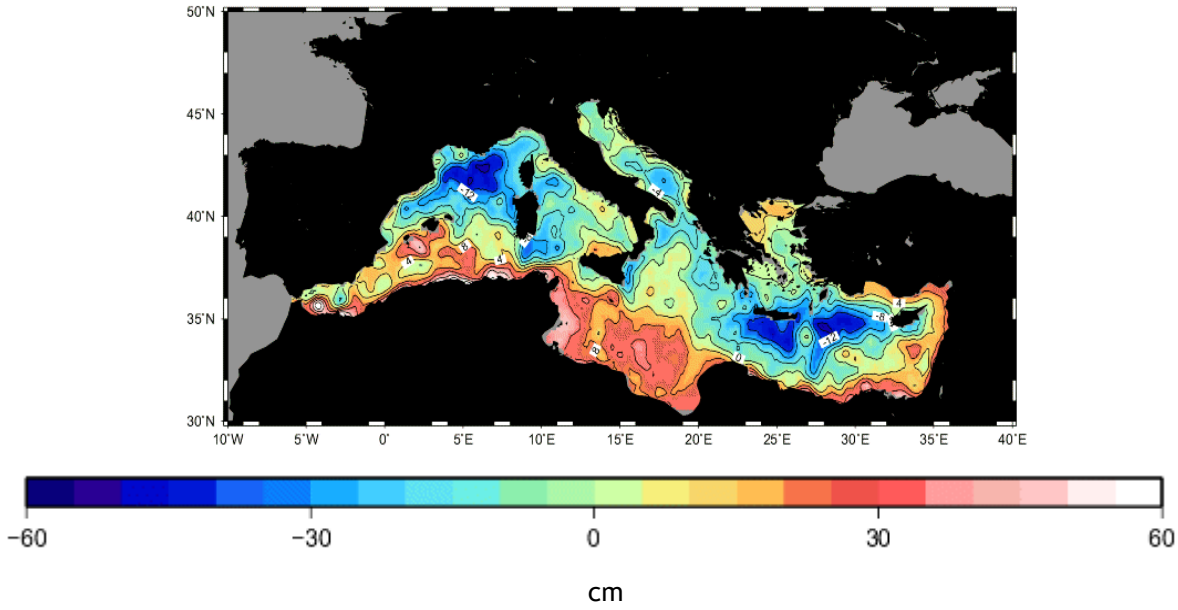

Figure 13:The SMDT07 computed by Rio et al, 2007 in the Mediterranean Sea

The drifting buoy velocities used to compute the mean circulation of Figure 14 have been processed and made available by Poulain et al, 2011. The drifting buoy velocities have been corrected for the wind-driven circulation to consider only the geostrophic component of the currents. Then the altimetric velocity anomalies have been interpolated along the drifter trajectory and subtracted from the drifter geostrophic velocity to estimate a set of synthetic mean velocities as was done in section 3 for the global ocean.

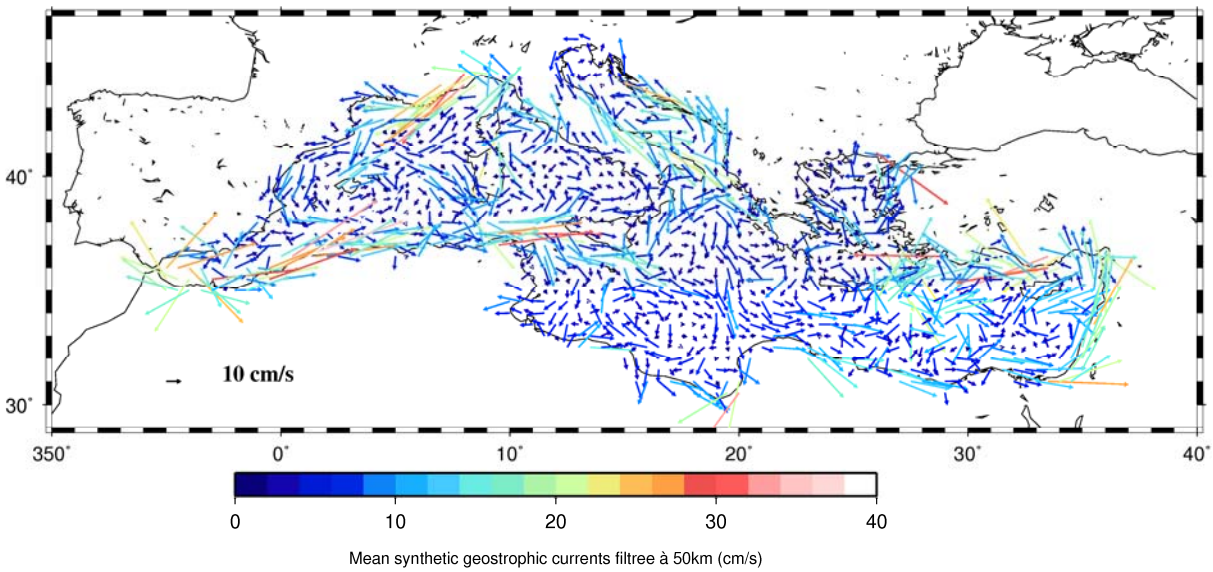

Figure 14: Synthetic velocities computed from drifting buoy velocities and altimetric velocity anomalies and averaged over 50 km.

Figure 15 shows the mean circulation of the Mediterranean Sea at 300km resolution for (top) the geodetic MDT computed from ITG-GRACE2010s, (middle) the geodetic MDT computed from EGM-DIR2 and (bottom) the synthetic velocities.

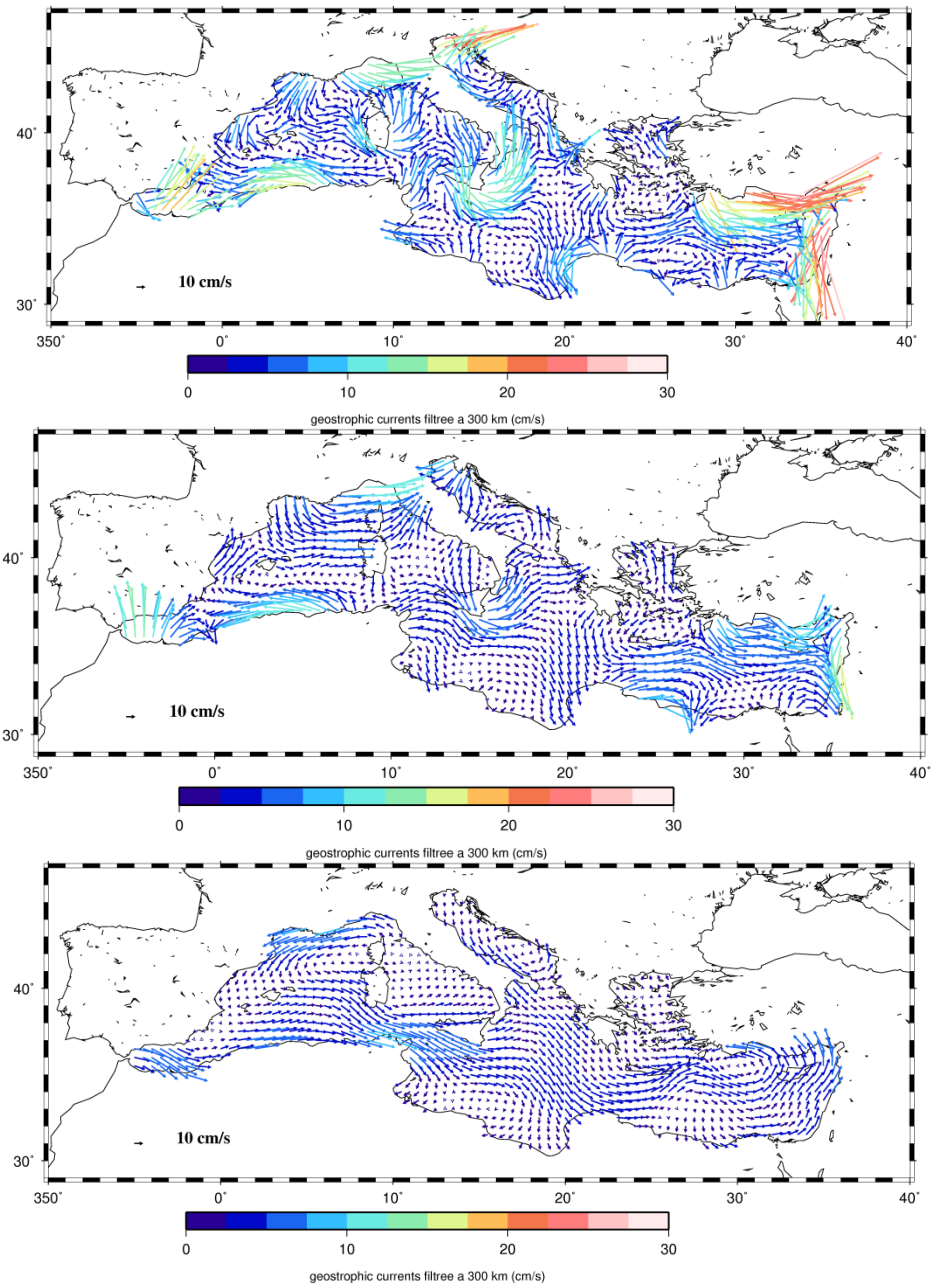

Figure 15: Mean geostrophic velocities in the Mediterranean Sea computed at 300km resolution from MSS minus ITG-GRACE2010s (top) MSS minus EGM-DIR2 (middle) and synthetic velocities as described in the text (bottom)

A quantitative assessment of the GOCE MDT accuracy compared to the GRACE MDT accuracy is finally shown on Figure 16. The standard deviation of the differences between the synthetic velocities and the geodetic MDT velocities at various resolution was computed for the zonal component (top) and the meridional component (bottom).

This plot shows that we obtain a strong reduction, at all spatial scales, of the standard deviation of the differences when the GOCE MDT is used instead of GRACE. However, the obtained STD values are far above the values obtained with the SMDT07 field. Moreover, the obtained STD values are far above the STD of the synthetic velocities themselves. This indicates that, although an improvement is obtained with GOCE data, the resulting solution is still by far dominated by geoid errors.

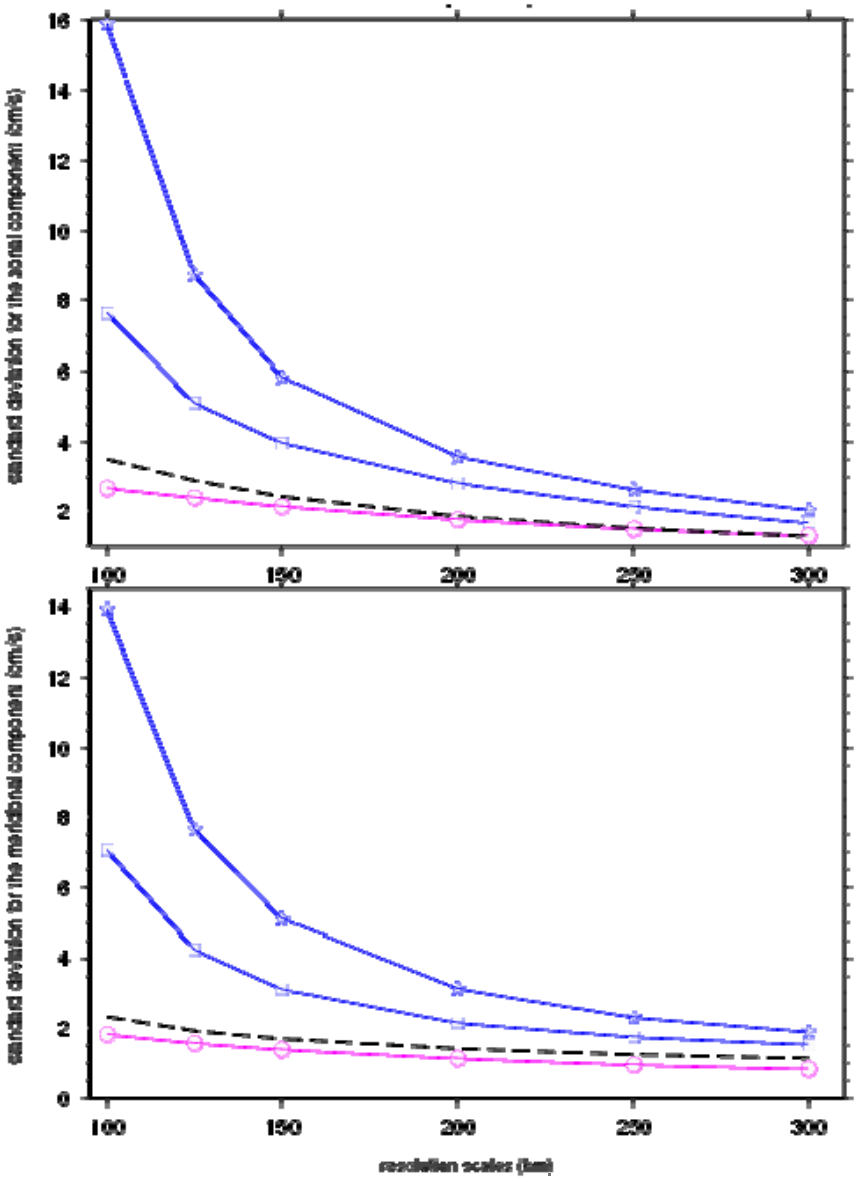

Figure 16: Standard deviation of the differences between the synthetic velocities and the mean geostrophic velocities computed from the geodetic MDTs both filtered at various length scales. Blue stars: geodetic MDT computed with ITG-GRACE2010s. Blue squares: geodetic MDT computed with EGM-DIR2. Pink circles: SMDT07. Dashed black line: standard deviation of the synthetic velocities.

To conclude, the present accuracy of the preliminary GOCE geoid models is not sufficient to be useful for retrieving the Mediterranean Sea mean circulation. In the future, we may try to use more sophisticated filters than the Gaussian filter applied here, in order to extract the maximum information from the GOCE geoid model. Also, the Mediterranean Sea may benefit from the next

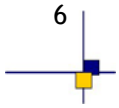

release of GOCE geoid models based on twice more data (one year) than the second HPF release. While the impact of these six supplementary months may be small in the strong western boundary currents of the global ocean, which are already well resolved by the use of the geoids from the second release, the Mediterranean Sea may be a very interesting test basin to focus on for validating the next ESA HPF release.

4. Regional zoom n°2: COMPARISON OF GOCE MDT TO NIILER'S MDT IN THE NORTH ATLANTIC OCEAN

4.1. INTRODUCTION

The current systems of the North Atlantic play an important role in the regulation of the Earth's climate. The GulfStream and its extension transport heat poleward from the equator, helping to maintain the relatively temperate climate of western Europe relative to similar latitudes in North America and Eastern Europe (*Rhines et al.*, 2008).The East Greenland Current carries freshwater from the Arctic into the Atlantic to maintain the freshwater balance between the Atlantic and the Pacific (*Woodgateet al.*, 1999). Given their importance in these respects, the accurate determination of the North Atlantic currents is highly desirable. In this section, we present an initial analysis of an MDT and associated currents derived from the different GOCE geoid models for the North Atlantic region. After briefly describing the data and methods in the next section, in Section 4.3 we considered the MDT signal up to degree and order (d/o) 180. In section 4.4 we ask if additional MDT signal can be recovered from the spherical harmonic terms beyond this d/o. Finally some brief conclusions are provided in section 4.5.

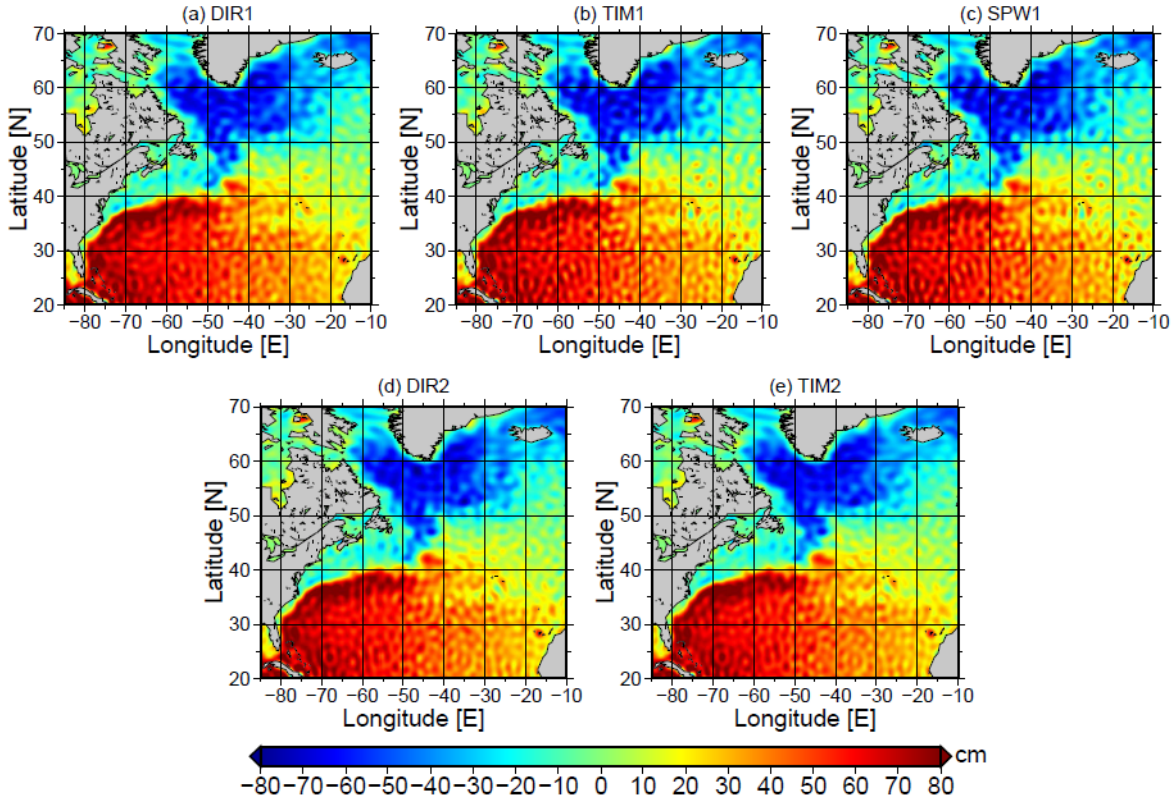

Figure 17: The North Atlantic mean dynamic topography (MDT) determined from the five GOCE gravity models released so far. The top row shows the first generation of models and the bottom row shows the second generation. MDTs are computed by the spectral method with truncation at degree and order 180. DIR, TIM, and SPW refer to the direct,timewise and spacewise approaches to obtaining the GOCE gravity models.

4.2. METHOD

The GOCE MDTs are calculated by subtracting the GOCE derived geoids from a mean sea surface (MSS). Here we use a MSS provided by CLS (Collecte Localisation Satellites) covering the period1993-1999 (*Hernandez and Schaeffer*, 2001). The MDTs are calculated using the spectral approach as described in *Bingham et al.* (2008). Removal of MDT noise is commonly achieved by spatial smoothing with a Gaussian or similar filter (e.g. *Tapley et al.*, 2003; *Jayne et al.*, 2003). However, as illustrated by (*Bingham et al.*, 2008), such *isotropic* filters,by filtering across MDT gradients have the undesired side-effect of drastically attenuating ocean currents calculated from the smoothed MDT. As demonstrated by *Bingham* (2010), an alternative filtering method based on anisotropic diffusion significantly reduces the problem of gradient attenuation, and loss of current resolution, by preferentially filtering along, rather than across, steep MDT gradients. Therefore this *anisotropic* filtering method is the one employed here.

4.3. MDTS TO DEGREE AND ORDER 180

We begin by considering MDTs computed to d/o 180.This is the maximum d/o of ITG2010S gravity model, considered, at the time of writing, to be the best satellite only GRACE solution. As such, it provides an important benchmark against which GOCE can be judged. Figure 17 shows the GOCE MDTs to d/o 180 for all of the available models. All of them capture the main features of the North Atlantic circulation. And all are, to some extent, contaminated with small scale noise, which, since we have used the spectral approach, comes mainly from geoid commission error. For this perspective there is little to distinguish the models. The currents speeds derived from the five models are shown in Figure 18.

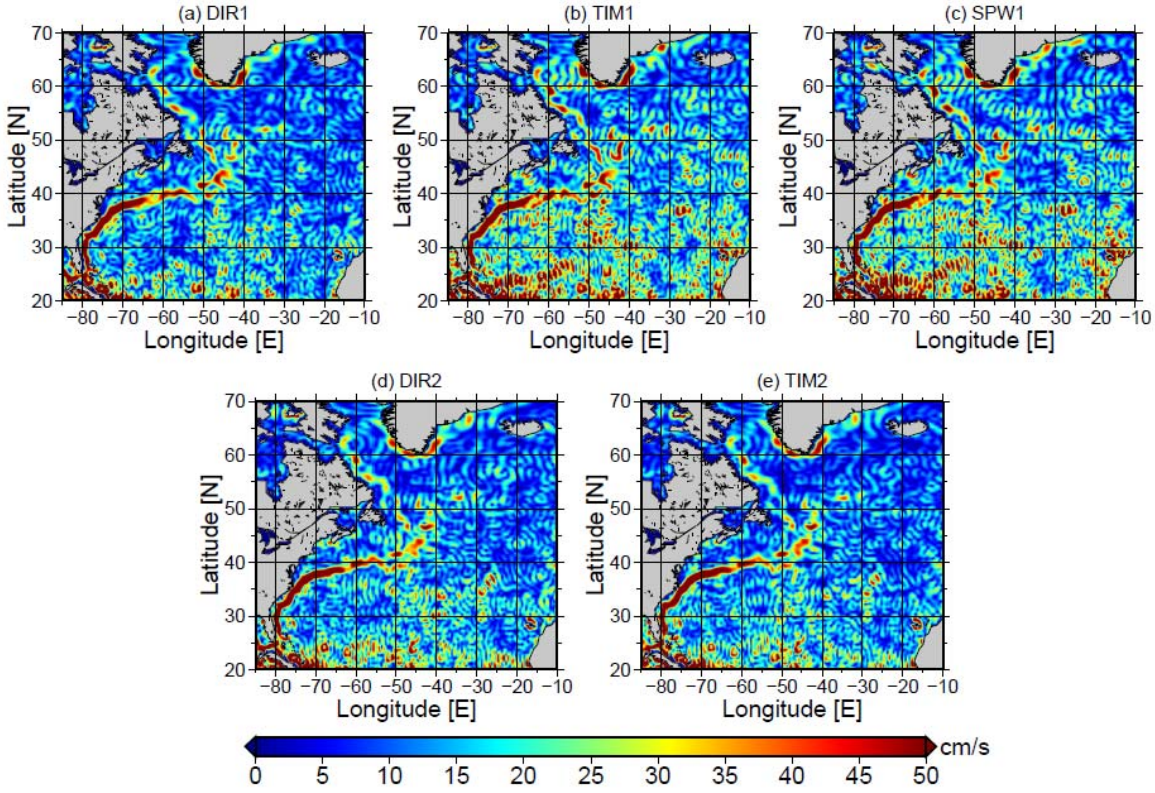

Figure 18: *Geostrophic current speeds obtained from the GOCE MDTs shown in* **Figure 17**

In all, the path of the Gulf Stream is clear, but, because the process of taking the gradient of the MDT to determine currents also amplifies small scale noise, differences between the models are now clearer. For the first generation of models, it is clear that the direct solution is much smoother than either the timewise or spacewise approaches. This is because the GRACE EIGEN5C gravity model, which also includes surface data, was used as an a priori constraint on the DIR1 solution. The DIR2 model does not use this constraint and for this reason the noise in the DIR2 MDT is little greater, even though the second release is based on three times more GOCE observations. The true impact of the additional data on the MDT calculation is seen by comparing the current maps for TIM1 and TIM2, where the processing method has remained consistent between releases. It is clear that the noise in the TIM2 MDT has been much reduced, and this is due to the reduced geoid commission error.If we quantify the noise in the geodetic MDTs by computingthe RMS residual between the currents obtained from the geodetic MDTs with those from the Niiler MDT (*Niiler et al.*, 2003), which is based solely on drifter data, over 10x10 degree tiles, then it is possible to determine the percentage reduction in noise of the GOCE MDTs compared with the GRACE MDT. This is shown in Figure 19. The improvement between first and second generation timewise solutions is clear, and for the latter, the noise has been reduced by up to 85% compared to the GRACE solution. Similar improvements are seen in the DIR1 and DIR2 MDTs. One poor area lies in the southwestcorner of the domain. Although, even here, noise has been reduced between the first and second releases of the timewise solution so that the TIM2 MDT is about 50% less noisy than the GRACE MDT under the metric specified. Incidentally, since the calculation method is the same in all cases, this shows that this is true geoid commission error rather than being merely numerical issues associated with the spectral calculation method. **Figure 20** shows the currents computed from the GOCE MDTs (to d/o 180) once the MDTs have been diffusively filtered. The number of iterations required in each case to minimise the RMS difference between the geodetic and Niiler MDTs, as defined above, are shown above the panels. This is the halting criterion for the filtering procedure, analogous to choosing the filter radius for a spatial averaging filter. As expected, the number of iterations is closely related to the noise in the unfiltered MDTs. Thus, the DIR1MDT required less filtering than the other two first generation models and there is little difference in the number of iterations required for the DIR1 and DIR2 MDTs, while, of the second generation models, the TIM2 MDT requires less filtering than the TIM1 MDT. From visual inspection alone there is little to distinguish the current maps in **Figure 20**. Therefore, in **Figure 21**, we compare the currents at nine locations, considered of oceanographic interest, as marked in **Figure 20**e. For comparison, also included are current speeds at the same location from Niiler and from the ITG2010S MDTs. Because the GRACE MDT is much more noise than any of the GOCE MDTs, it requires much more filtering (235 iterations). We should expect, therefore, that in general the GRACE currents will be more attenuated than those from GOCE. With the exception of location 8, were the current speeds are similar due to residual noise in the GRACE MDT boosting the current estimated from GRACE here, this is just what we find; at all other locations the*.cur*rents speeds from the GOCE MDTs are, by varying degrees, greater than those from GRACE. For locations 2and 3 along the Gulf Stream the difference is greater than 20 cm/s. The most marked difference with the Niiler currents is at location 1. Because of the path taken by the current here through a narrow passage this is a challenging current for the filtering method to preserve. At the other locations the agreement between Niiler and the GOCE currents is remarkable good. Surprisingly, perhaps, at four locations the currents from GOCE exceed those based on the in-situ data. At location 7, which samples the West Greenland Current, where the difference is most marked, this seems to result from the Niiler estimate failing to properly capture the current along this coastline. This may be due to sparse sampling in this ice prone region. Location 5, corresponds to the North Atlantic Current, and the difference here seems to result from this current being better resolved in the GOCE estimates. Finally ,at location 3, the Niiler estimate seems too weak by about 10 cm/s. The reader will note, however, there does not seems to be systematic differences between the GOCE estimates, in so far as there is not a clear relationship between the number of iterations required to filter each MDT and the relative strength of the currents derived from it. This would suggest that any differences in current speeds due to 20 iteration range among the GOCE MDTs cannot be resolved against the impact noise may have on the filter.

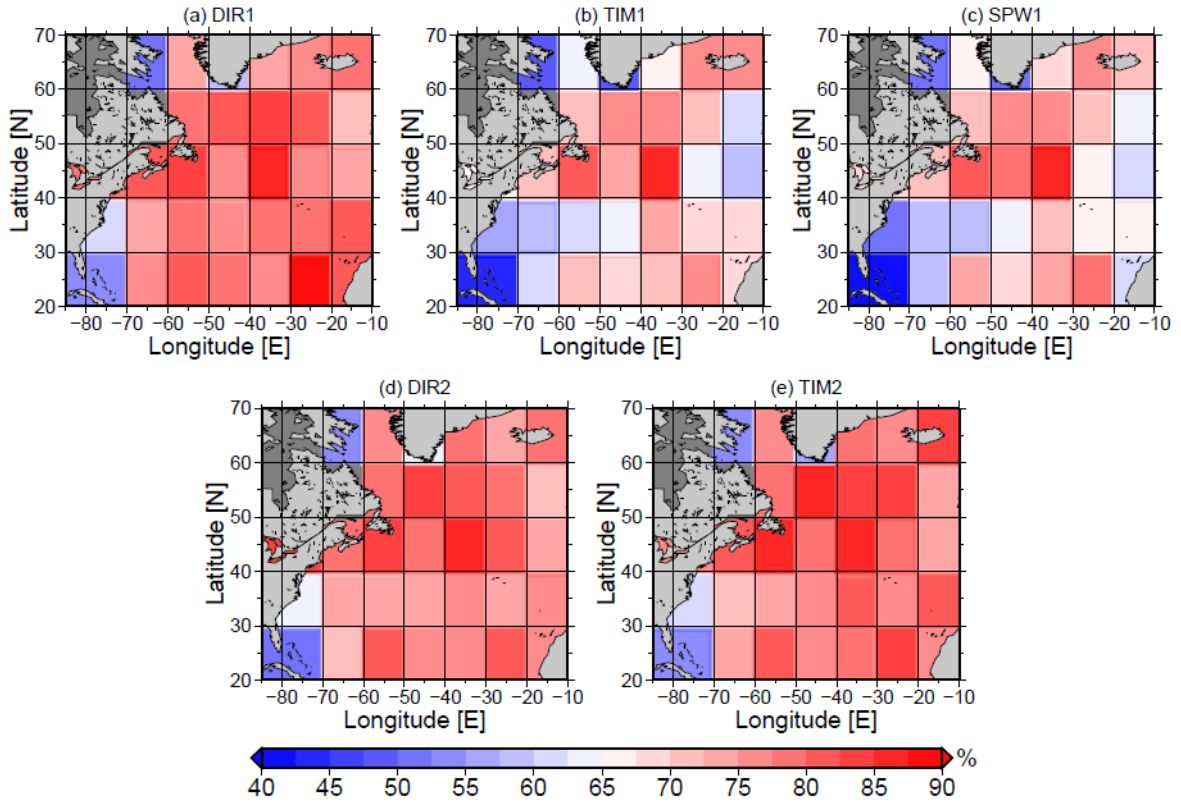

Figure 19: The reduction in the noise of the GOCE MDTs relative to the GRACE ITG2010S MDT, where noise is here defined as the RMS difference, computed over the 10x10 tiles shown, between the currents obtained from the geodetic MDTs and the currents from the Niiler drifter-only MDT.

4.4. GOING BEYOND DEGREE AND ORDER 180

In the previous section we limited all of the MDTs to d/o 180, even though more spherical harmonic terms are available for each of the GOCE gravity models. This essentially showed that the reduced noise in all of the GOCE MDTs due to reduced geoid commission error in the GOCE gravity models, compared with the noise in the GRACE MDT, enabled a better estimate of ocean currents because less noise entailed less filtering, and therefore less attenuation of ocean currents. Yet, the noise differences between the GOCE MDTs themselves were not great enough to change how well the ocean currents could be resolved. We now consider whether the additional spherical harmonic terms that are available in the GOCE gravity models can be used to improve further the estimated currents. Presently, the TIM2 MDT is given to the highest degree and order (250). **Figure 22** shows ocean current speeds from TIM2 MDTs computed in 10 d/o intervals from d/o180 to d/o 250. *Bingham et al.* (2011) show how geoid commission errors grow with increasing d/o of truncation. **Figure 22** clearly demonstrates how this geoid commission error leads to increasingly noisy current speeds as the truncation d/o is increased, such that at d/o 210 the noise, particularly at lower latitudes, has a similar magnitude to the currents we are trying to resolve. At d/o 250, even the Gulf Stream cannot be resolved against the noise. From the discussion above, it should be clear that as the d/o is increased, the number of filter iterations require to minimise the RMS difference with the independent Niiler estimate is going to grow. The question is, therefore, at what point does this requirement for ever more severe filtering, negate any advantage to be had, in terms of additional signal, from the extra spherical harmonic terms? Reflecting the visual impression from **Figure 22**, the average RMS residual prior to filtering for the currents determined for the TIM2 MDTs grew from

17 cm/s at d/o 180to 64 cm/s at the maximum d/o of 250. In line with this, the number of iterations required to minimise the RMS difference between the geodetic currents and the Niiler currents rose from 96 to 191, with the finally obtained residual maintaining a relatively constant value of about 9 cm/s. From a visual inspection alone of the current speed maps (not shown) derived from the filtered MDTs there is little to distinguish between them over the range of truncations shown in **Figure 22**. We, therefore turn again to a comparison of current speeds at the nine locations described above. Again a systematic pattern, showing a clear and consistent d/o threshold that maximises the current speed is not obvious. If, however, we consider only those locations (1, 2 and 8) where the GOCE estimates are always lower than the in-situ estimate, then closer agreement, that is, the maximum current strength, is found at d/o 190 or d/o 200 (second or third bars). For the location where the GOCE estimates span the in-situ estimate.(3, 4, 5, and 9), with the exception of location 9, the maximum current speed is found between d/o 200 and d/o220. For the two locations where the GOCE estimate always exceeds the in-situ estimate (locations 5 and 7) and location 9, the maximum strength is attained for d/o 180.Taken together these suggest an optimum truncation of about d/o 200, and this is confirmed by visual inspection. Yet, it is clear from**Figure 23**, that for all of the locations considered, the difference between the currents obtained with truncation at d/o 180 and those obtained at the maximizing d/o is quite small, the largest difference of about15 cm/s being at location 4 - corresponding to the Mann Eddy.

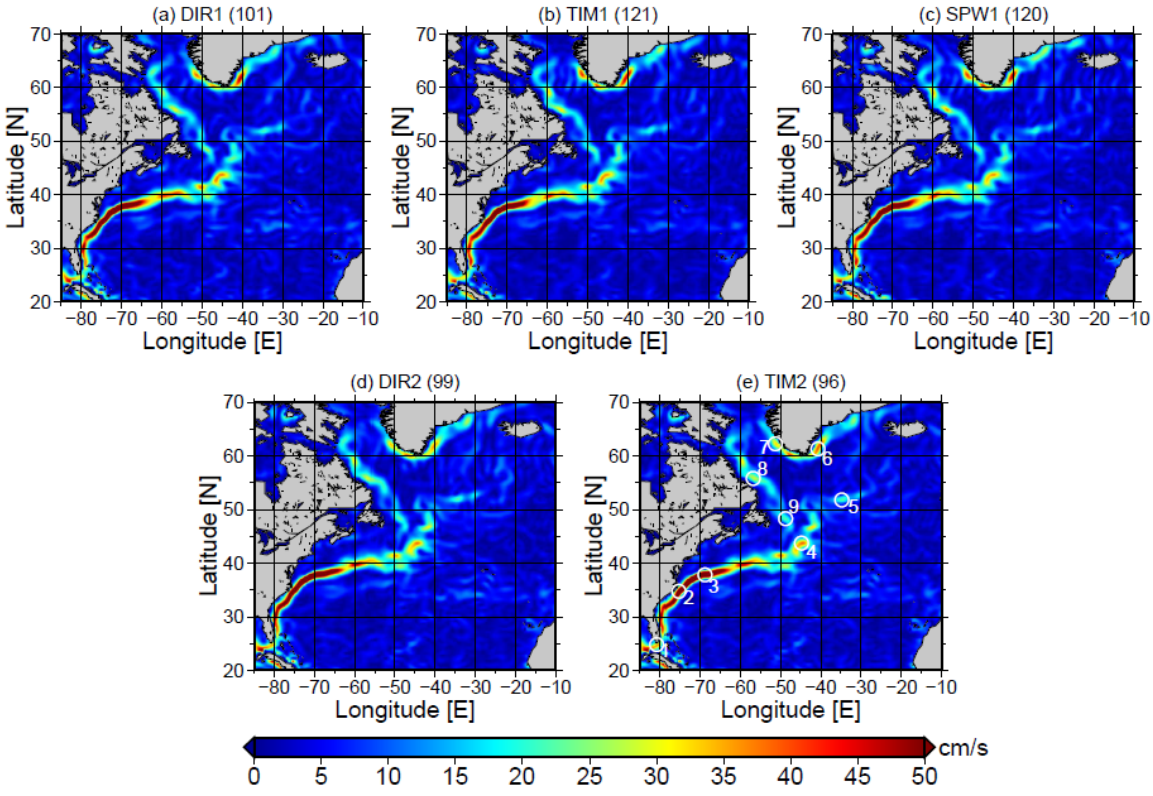

Figure 20: Geostrophic current speeds obtained from the GOCE MDTs shown in Figure 16 **once the MDTs have been diffusively filtered as described in the text. The number of iterations required to minimise the RMS difference with the Niiler MDT are shown above each panel.**

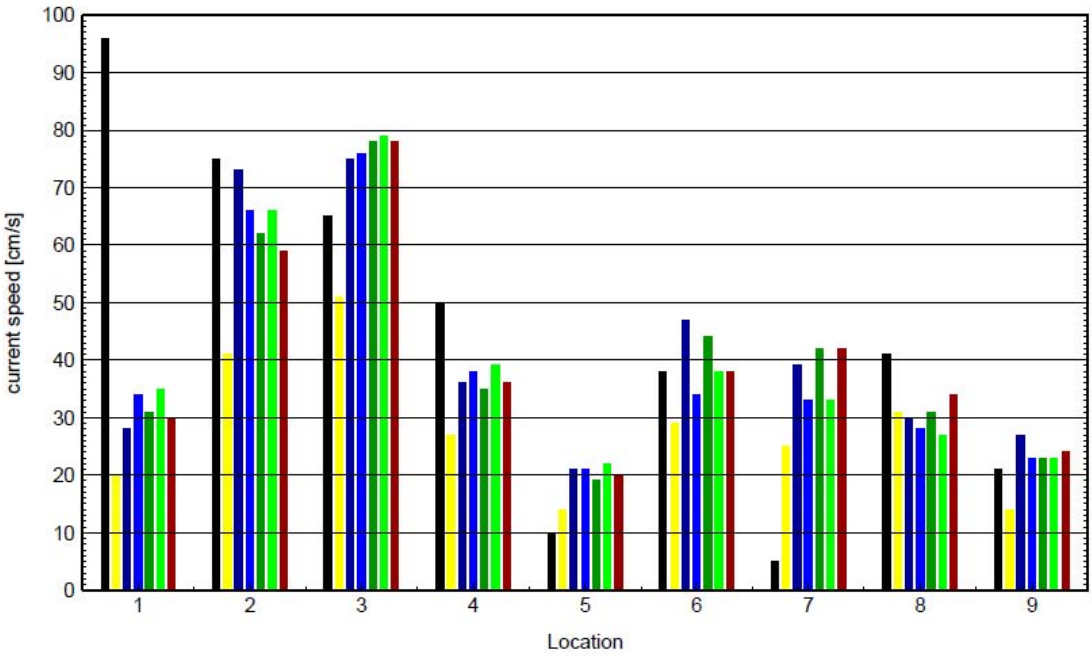

Figure 21: A comparison of current speeds obtained from the diffusively filtered MDTs shown in Figure 20 at the nine locations marked in Figure 20e. DIR1 (dark blue), DIR2 (blue), TIM1 (dark green), TIM2 (green), SPW1 (dark red). Currents at the same locations from the Niiler drifter only MDT are shown in black (no filtering), and the currents from the diffusively filtered GRACE ITG2010S MDT are shown in yellow.

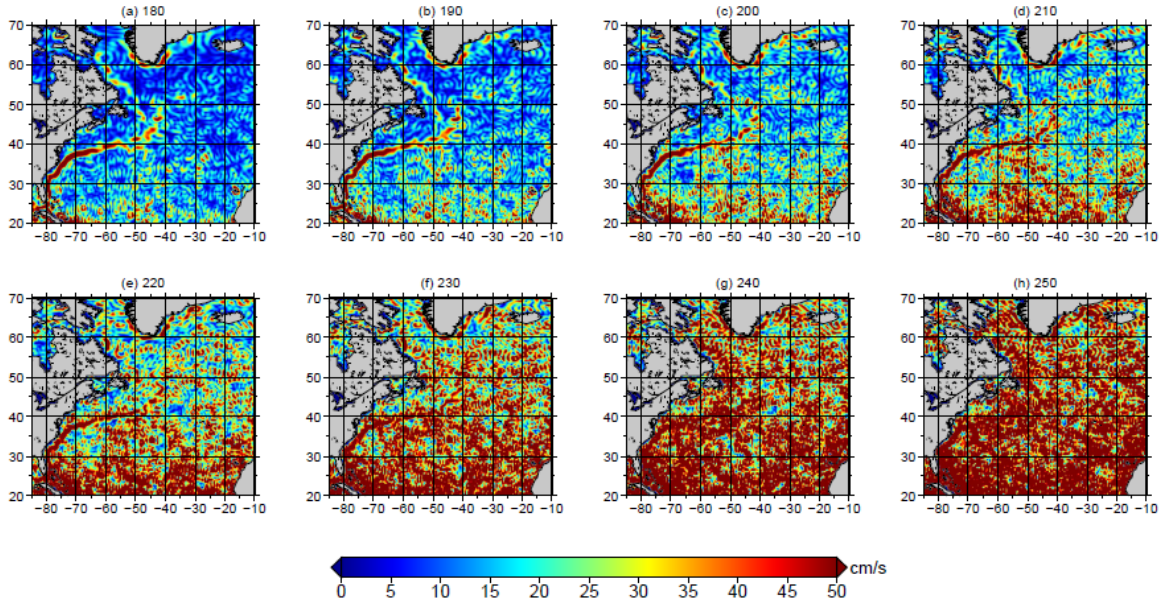

Figure 22: Geostrophic current speeds obtained from unfiltered TIM2 MDTs over a range of truncations as shown above the panels.

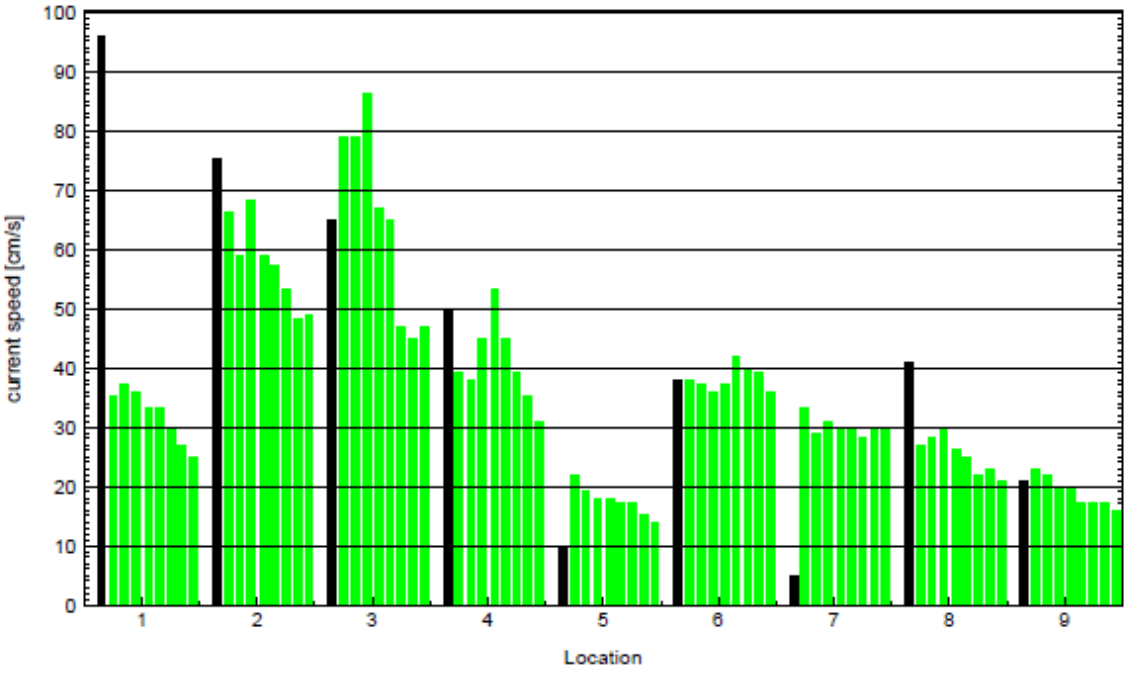

Figure 23: A comparison of current speeds, at the nine locations marked in Figure 20e, obtained from the TIM2MDTs shown in Figure 22 once diffusive filtering has been applied. The leftmost bar at for each location represents the currents from the MDT truncated at d/o 180 while the rightmost represents the MDT truncated at d/o 250, with a 10 d/o increment between successive bars. Currents at the same locations from the Niiler drifter-only MDT are shown in black (no filtering).

4.5. CONCLUSIONS

In this section we have compared the first five GOCE gravity models in terms of the mean North Atlantic circulation that can be derived from them. Because the high degree commission errors of all of the GOCE models are lower than those from the best satellite-only GRACE solution, all of the derived GOCE MDTs are much less noisy than the GRACE MDT. This is especially evident when currents rather than heights are considered, as in taking the height derivative we amplify the short scale noise. Quantifying the noise in the geodetic MDTs against the Niiler drifter-only MDT we find that for the second generation of GOCE models, based on 6 months of data, noise is reduced by between 40% and 80% compared with the best satellite only GRACE model. They therefore require less severe filtering and, as a consequence, the strength of the currents calculated from them are in better agreement with those from an in-situ drifter based estimate. Because the processing has remained consistent between the first and second generations of the timewise models, it is possible to demonstrate that the reduction in MDT noise from the additional data in the second release is substantial. However, given that some filtering is still required, this translates into only a small improvement in ocean currents. That the improvement in terms of ocean currents between the first and second solutions is ultimately rather small, is partly a reflection of both the strength and limitations of the filtering method employed. Firstly, the diffusive filtering method employed is very successful at finding and preserving the gradients in the underlying MDT while removing the background noise, particularly for strongest currents such as the Gulf Stream. Therefore, if we restrict ourselves to a fixed degree and order such as 180, as we have done above in section 4.3, then despite the greater noise in the first generation models compared to the second generation, the filter can still effectively remove this noise without much additional effort, and the underlying gradients are preserved. Only when the noise is much greater, as it is for the GRACE estimate, does the additional effort by the filter result in substantial degradation of the signal. The limitation of the filter reveals itself as we move beyond degree and order 180. At degree and order 250,for

example, we expect the *MDT* omission error to have been reduced. Due the error characteristics of the gravity model, however, at d/o 250 the noise as grown substantially. A perfect filter would remove this noise while preserving the additional signal. With the filter employed here, we find a threshold at about d/o 210, beyond which the rise in noise, and the additional burden it places on the filter, means no additional signal can be extracted. So, although the diffusive filter is much more effective than simple Gaussian filtering, a more sophisticated filter, perhaps taking into account the error variance covariance information provided with the GOCE gravity models, may be required, as things stand, to extract the additional MDT signal present in the higher order terms. Of course, as the data record grows the noise may come down to a level at which any additional signal can be obtained without the need for advanced post-processing methods.

5. COMPARISON OF GOCE MDT TO HYDRODYNAMICAL MODELS

5.1. The ECCO/GECCO hydrodynamical models

In this section, we have inter compared GRACE and GOCE based Mean Dynamic Topographies (MDTs) and the corresponding surface geostrophic currents to two hydrodynamic model integrations. Both integrations use the Massachusetts Institute of Technology general circulation model (MITgcm; Marshall et al. [1997]) with essentially the same configuration, and the 4DVar assimilation method to bring the model into consistency with available hydrographic and satellite data as well as prior estimates of surface fluxes. Both models provide a MDT on a 1°x1° grid for the region 80°N - 80°S. The major difference of the two model runs is the different integration periods. While ECCO is integrated for the 11 years period 1992-2002, GECCO is a 50 years run (1952-2002). Details on the models can be found in Köhl et al. (2007) for ECCO and Köhl and Stammer (2008) for the GECCO synthesis.

From the model syntheses we use the time window 1993-1999 to compute the MDT. This means, that no re-referencing is needed when using the CLS10 Mean Sea Surface (MSS). Only for the second MSS, the DNSC08, we apply Sea Level Anomaly (SLA) to re-reference to the 1993-1999 time frame.

5.2. Computation of satellite-based MDT

The computation of 'geodetic' MDTs, as based on the difference of MSS and a geoid, is done in two steps. First, the MSS is transformed to spectral space and cut at degree and order (d/o) of the geoid (spectral filtering). Second, after having transformed the MSS back to physical space, and synthesized the geoid to highest available d/o, both on a 1/4° grid, the difference of the (filtered) MSS and the geoid is computed and spatially smoothed applying a Gaussian kernel. Degree-1 Stokes coefficients, which are missing in the GOCE geoid solutions, are obtained from the ITG-GRACE2010s geoid. The list of MDT solutions together with the applied filter is provided in Tab. 1.

For all GOCE based MDT we have used the CNES-CLS10 MSS. For the GRACE based MDT, both the CNES-CLS10 and the DNSC08 MSS have been used resulting respectively in the GRACE-CLS and the GRACE-DNSC MDT solutions.

Table 1: List of geodetic MDTs used in this section.

Name of geodetic MDT	geoid	max. d/o	MSS	Gaussian filter
GOCE-DIR	GOCE-DIR	240	CLS10	1.4°
GOCE-TIM	GOCE-TIM	224	CLS10	1.8°
GOCE-SPW	GOCE-SPW	210	CLS10	1.8°
GOCE-DIR-2	GOCE-DIR, 2nd Release	240	CLS10	1.2°
GOCE-TIM-2	GOCE-TIM, 2nd Release	250	CLS10	2.0°
GOCO	GOCO01s	224	CLS10	1.2°
GRACE-CLS	ITG-GRACE2010s	180	CLS10	2.0°
GRACE-DNSC	ITG-GRACE2010s	180	DNSC08	2.0°

Since the hydrodynamic models are restricted to the region between 80°N and 80°S, and the MSS have large uncertainties in (temporarily) ice-covered areas, we restrict all comparisons to the region defined by the models. We also apply the 1° (G)ECCO grid for all comparisons since this grid defines the highest spatial resolution available in all MDTs we use in our study.

Table 2: Global mean standard deviation (upper right triangle) and R.M.S. (lower left triangle) of differences in the listed MDTs. In the diagonal, the R.M.S. of the MDT signal is included.

\ std.dev., [mm]	GOCE DIR	GOCE TIM	GOCE SPW	GOCE DIR-2	GOCE TIM-2	GOCO	GRACE CLS	GRACE DTU	ECCO	GECCO
R.M.S. \										
GOCE-DIR	**707**	16	13	11	18	11	17	26	73	100
GOCE-TIM	16	**708**	11	20	11	19	13	23	72	100
GOCE-SPW	13	11	**706**	18	11	18	10	22	71	98
GOCE-DIR-2	11	20	18	**708**	23	8	22	29	75	102
GOCE-TIM-2	18	11	11	23	**705**	23	9	23	72	98
GOCO01s	11	19	18	8	23	**710**	22	28	74	102
GRACE-CLS	17	13	10	23	9	22	**705**	20	71	97
GRACE-DTU	27	26	24	30	25	30	23	**633**	68	88
ECCO	73	72	71	75	72	74	71	68	**732**	68
GECCO	100	100	98	102	98	102	97	88	68	**699**

Table 3: Area-weighted global mean difference of listed MDTs (row - column).

global average [mm]	GOCE TIM	GOCE SPW	GOCE DIR	GOCE DIR-2	GOCE TIM-2	GOCO	GRACE CLS	GRACE DTU
GOCE-TIM		0.8	0.7	-0.2	1.4	0.1	0.4	-10.8
GOCE-SPW	-0.8		-0.1	-1.0	0.5	-0.7	-0.4	-11.4
GOCE-DIR	-0.7	0.1		-0.9	0.6	-0.6	-0.3	-11.6
GOCE-DIR-2	0.2	1.0	0.9		1.5	0.3	0.6	-10.6
GOCE-TIM-2	-1.4	-0.5	-0.6	-1.5		-1.2	-0.9	-12.3
GOCO01s	-0.1	0.7	0.6	-0.3	1.2		0.3	-10.7
GRACE-CLS	-0.4	0.4	0.3	-0.6	0.9	-0.3		-11.4

GRACE-DTU	10.8	11.4	11.6	10.6	12.3	10.7	11.4

5.3. MDT spatial variability

To discuss the spectral content of the MDT products, a spherical harmonic analysis is performed. To perform the analysis, the OBP maps have to be globalized. This is done by solving numerically the Laplace Equation for the land grid points as a Dirichlet problem with the ocean coastal values as boundary values. This results in an as smooth as possible mapping over land to minimize the influence of land signals in the spectrum. Figure 24 displays the square root of the degree variances in the top and the cumulated degree variance in the bottom panel.

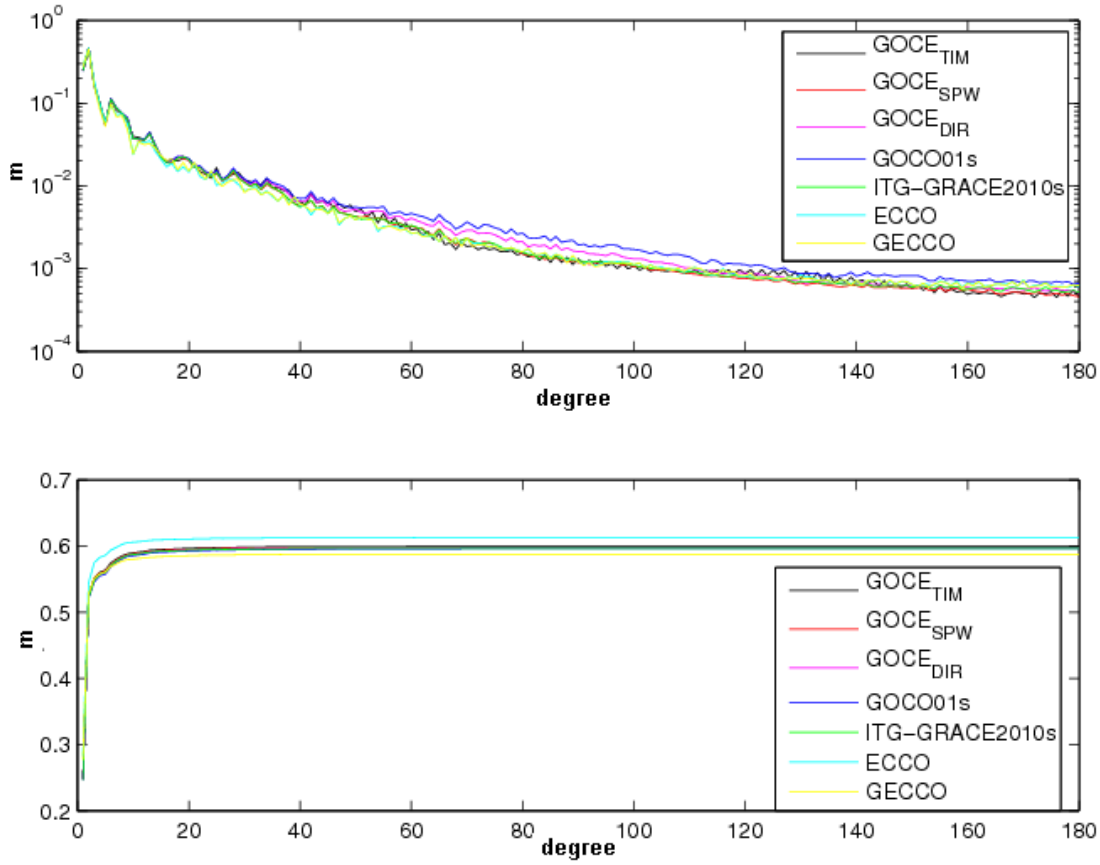

Figure 24: Spectral analysis of MDTs listed in the legend. (top) Square root of degree variances (m), (bottom) cumulated square root of degree variances (m).

All products largely agree in the overall spatial variability (60 cm) and also for the separation into different length scales. There is a slightly higher signal strength for the GOCO and the GOCE-DIR models for degrees larger than 50 (400 km and shorter wave lengths). Note, that the R.M.S. values provided in the diagonal of Tab. 2 are not directly comparable to the 60 cm variability found from the spectral analysis, since the R.M.S. is restricted to the ocean and is computed from a simple

average of variances at each grid point, no down-weighting for grid points in high latitudes is applied.

5.4. GOCE MDTs

The statistics of the differences between all MDTs in our study and specifically those obtained from all 5 currently available GOCE solutions are provided in Tables 2 and 3. The mapped MDT differences obtained from the newest GOCE solutions from the three different methods (GOCE-DIR-2, GOCE-TIM-2, GOCE-SPW) is shown inFigure 24. No strong long-scale differences are found between the GOCE-MDTs. The global mean offset between different maps is 3.0 mm or less (see Tab. 3). The correlation is larger 0.99 for all comparisons. The strongest differences (R.M.S. of 24 mm) are between the GOCE-TIM-2 and the GOCE-DIR-2 products, the MDTs with the longest (2°) and shortest (1.2°) length scale of the spatial filter applied. In this difference the regions with strong gradients in MDT emerge, as the Kuroshio and Gulf Streams, and the ACC. The closest agreement (R.M.S. of 10 mm) is found for the two DIR products.

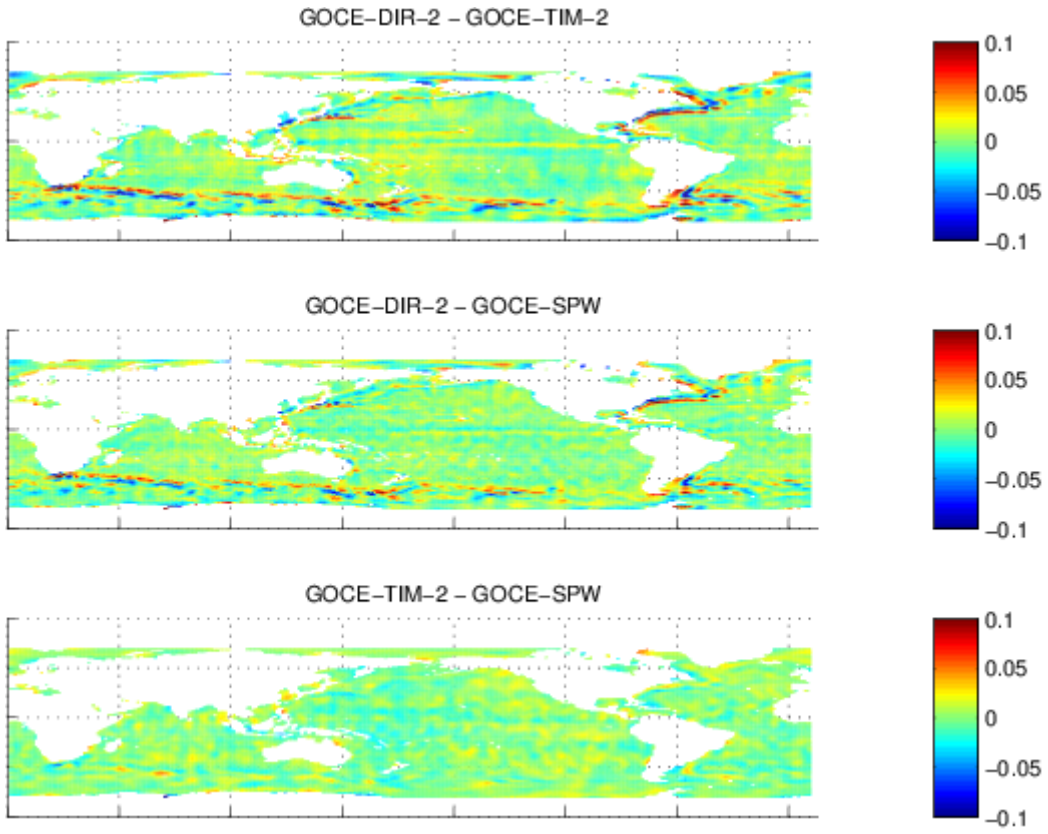

Figure 25: Differences in GOCE-MDTs (m).

The spherical harmonic analysis (with setting land values to zero, see Figure 25) shows, that the differences in the GOCE MDTs are of comparable magnitudes up to some degree 20 (1000 km length

scale) and diverge for shorter length scales, mainly in dependence of the differences in the cut-off length length of the applied spatial filters. The only exception is the comparison of the two DIR solutions, which closely agree for large spatial scales. In Figure 24, top, we included also the signal strength of the GOCE-DIR MDT for comparison with the disagreement of the GOCE MDT maps. It is clear from the figure, that the signal strength is overall much larger than the discrepancies (approximately 20 mm compared to 700 mm variability, see Tab. 2). Up to approximately degree 20 (1000 km) the differences are at least one order of magnitude smaller than the signal, and the signal remains larger than the differences up to some degree 130 (150 km).

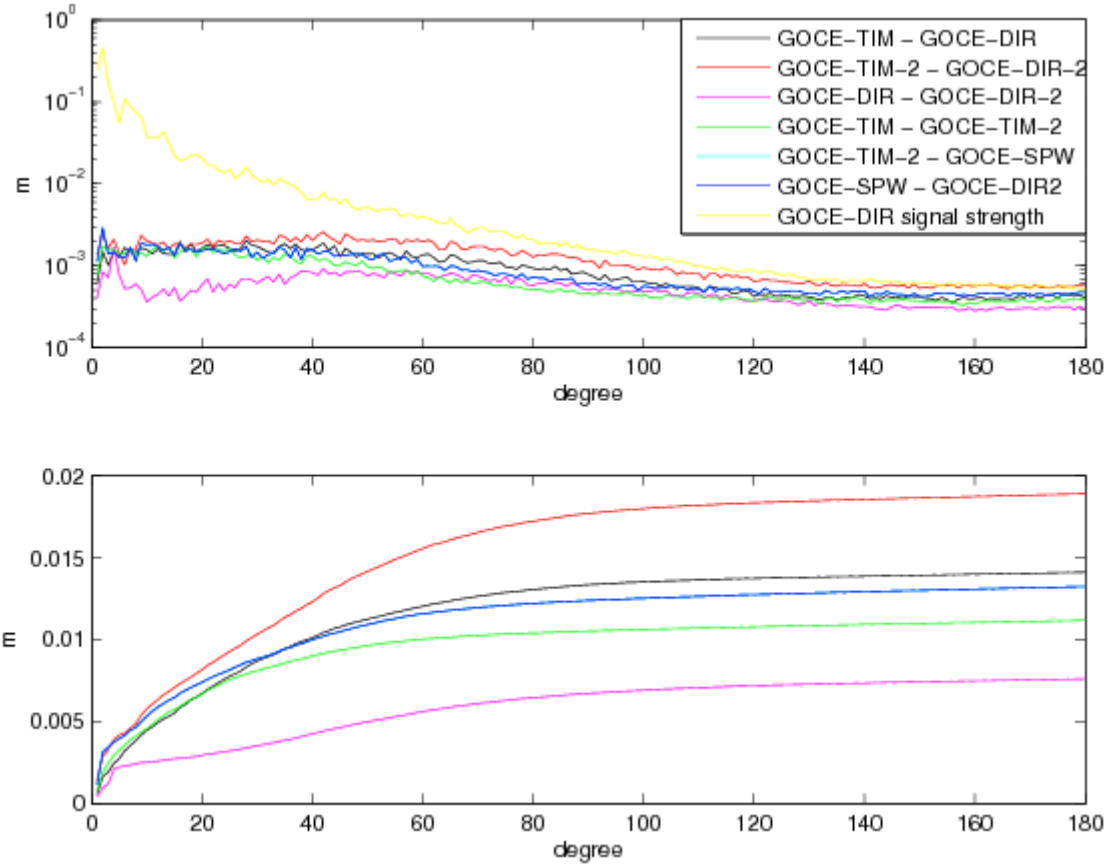

Figure 26: Spectral analysis of GOCE-MDT differences. (top) Square root of degree variances (m); the signal strength of GOCE-DIR is added for comparison (see Fig. 2). (bottom) cumulated square root of degree variances.

The difference in geostrophic surface currents is displayed in Figure 27 and Figure 28 for the *U* and *V* component, respectively. The differences are on short latitudinal-scale zonal stripes with strongest values near the equator, where *f* is small and thus, when calculating geostrophic currents, sensitivity to differences in the MDT gradients is highest. Global mean differences (Tabs. 4 and 6) are 0.3 mm/s or lower for all comparisons and both directions. *U* and *V* components generally look similar (see Tabs. 5 and 7), though discrepancies in *V* are generally larger. In contrast to the MDT, differences in the currents are much larger compared to the signal strength. For the *U* component the differences are approximately one fourth, for *V* approximately half of the signal. The smallest differences and highest correlations are found when comparing the GOCE-TIM and GOCE-SPW MDT

maps (5 mm/s and 1.00 for *U*, and 7 mm/s and 0.99 for *V*), while GOCE-DIR-2 and GOCE-TIM-2 have the highest discrepancies and lowest correlations in both directions (22 mm/s and 0.94 for *U*, and 45 mm/s and 0.90 for *V*).

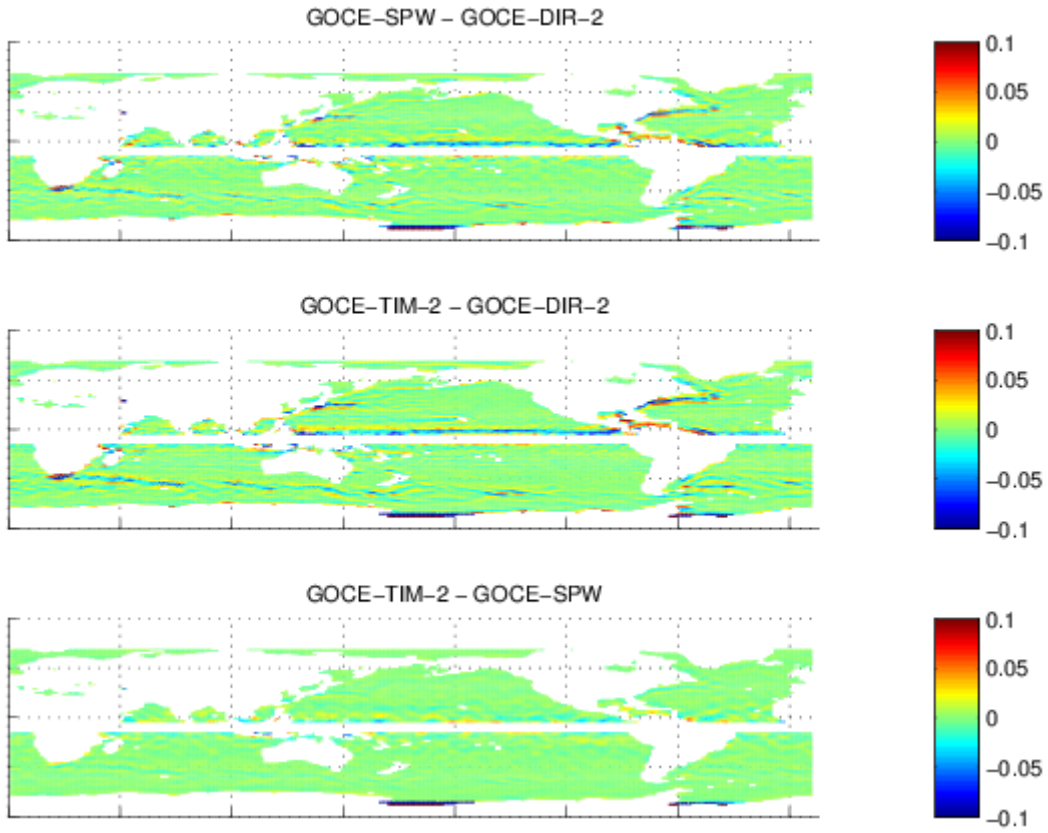

Figure 27: Differences in zonal geostrophic surface currents (m) for the GOCE MDTs.

Table 4: Global mean differences (upper right triangle; row - column) and correlations (lower left triangle) of zonal geostrophic currents for the listed MDTs.

\ mean difference [mm/s]	GOCE DIR	GOCE TIM	GOCE SPW	GOCE DIR-2	GOCE TIM-2	GOCO	GRACE CLS	ECCO	GECCO
Correlation \									
GOCE-DIR		-0.1	0.2	0.0	0.4	-0.1	0.2	0.8	-0.4

GOCE-TIM	0.99		0.2	0.1	0.5	0.0	0.3	0.8	-0.4
GOCE-SPW	0.98	1.00		-0.2	0.3	-0.3	0.0	0.6	-0.6
GOCE-DIR-2	0.99	0.98	0.97		0.4	-0.1	0.2	0.8	-0.4
GOCE-TIM-2	0.98	0.99	0.99	0.97		-0.5	-0.2	0.3	-0.9
GOCO01s	0.98	0.97	0.97	0.99	0.96		0.3	0.9	-0.3
GRACE-CLS	0.98	0.99	0.99	0.96	0.99	0.96		0.6	-0.7
ECCO	0.82	0.82	0.83	0.81	0.83	0.80	0.83		-1.6
GECCO	0.85	0.86	0.86	0.84	0.86	0.83	0.86	0.96	

Table 5: Global mean standard deviation (upper right triangle) and R.M.S. (lower left triangle) of differences in zonal geostrophic currents for the listed MDTs. In the diagonal, the R.M.S. of the velocity is included.

\ std.dev., [mm/s]	GOCE	GOCE	GOCE	GOCE	GOCE	GOCO	GRACE	ECCO	GECCO
R.M.S. [mm/s] \	DIR	TIM	SPW	DIR-2	TIM-2		CLS		
GOCE-DIR	**61**	10	11	9	13	11	13	36	32
GOCE-TIM	10	**58**	5	15	6	15	8	35	31
GOCE-SPW	11	5	**57**	15	7	16	8	35	31
GOCE-DIR-2	9	15	15	**64**	17	7	18	39	35
GOCE-TIM-2	13	6	7	17	**56**	18	6	35	30
GOCO01s	11	15	16	7	18	**65**	19	39	36
GRACE-CLS	13	8	8	18	6	19	**56**	35	30
ECCO	36	35	35	39	35	40	35	**67**	18
GECCO	32	31	31	35	30	36	30	18	**65**

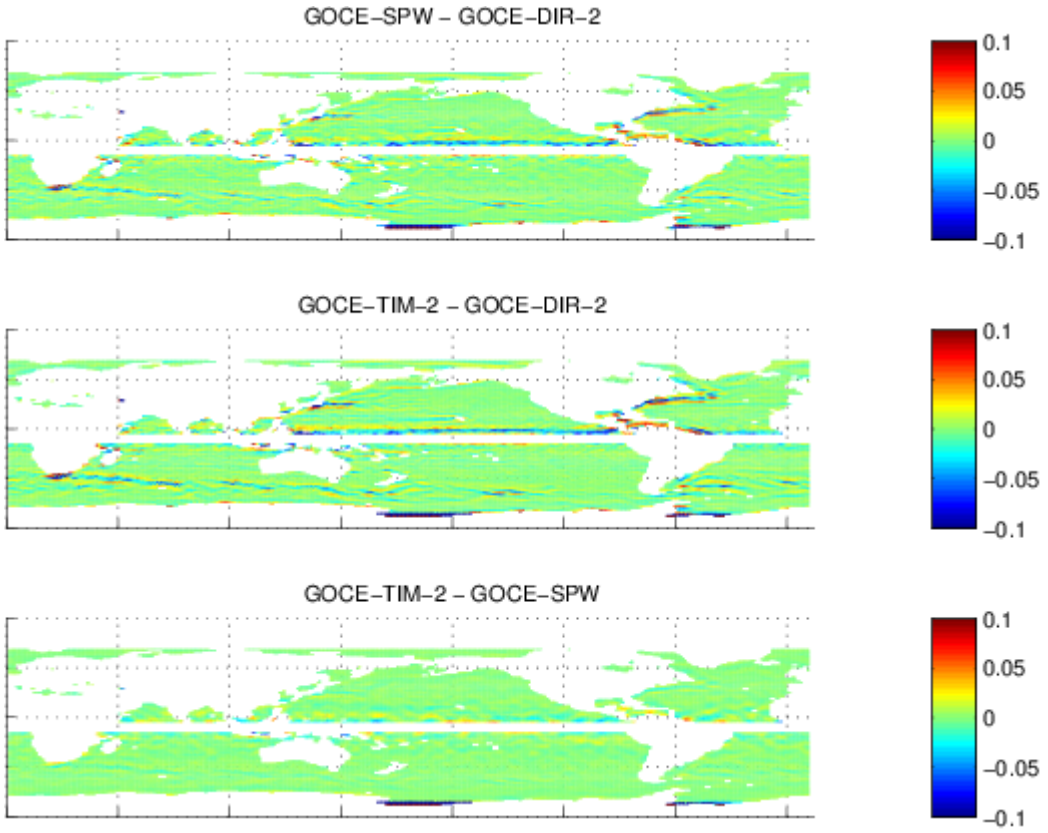

Figure 28: Differences in meridional geostrophic surface currents (m) for the GOCE MDTs.

Table 6: Global mean differences (upper right triangle; row - column) and correlations (lower left triangle) of meridional geostrophic currents for the listed MDTs.

\ mean difference [mm]	GOCE	GOCE	GOCE	GOCE	GOCE	GOCO	GRACE	ECCO	GECCO
Correlation \	DIR	TIM	SPW	DIR-2	TIM-2		CLS		
GOCE-DIR		0.0	0.0	-0.1	0.0	-0.2	0.1	0.6	0.3
GOCE-TIM	0.89		0.0	-0.1	0.0	-0.2	0.0	0.6	0.3
GOCE-SPW	0.90	0.94		-0.1	0.0	-0.2	0.1	0.6	0.3
GOCE-DIR-2	0.93	0.86	0.87		0.0	-0.1	0.1	0.7	0.4

GOCE-TIM-2	0.89	0.94	0.93	0.87		-0.1	0.1	0.6	0.3
GOCO01s	0.92	0.87	0.87	0.95	0.87		0.2	0.8	0.5
GRACE-CLS	0.90	0.91	0.92	0.86	0.94	0.87		0.5	0.2
ECCO	0.54	0.51	0.53	0.53	0.52	0.53	0.54		-0.3
GECCO	0.58	0.55	0.57	0.57	0.56	0.57	0.58	0.95	

Table 7: Global mean standard deviation (upper right triangle) and R.M.S. (lower left triangle) of differences in meridional geostrophic currents for the listed MDTs. In the diagonal, the R.M.S. of the velocity is included.

\ std.dev., [mm/s]	GOCE	GOCE	GOCE	GOCE	GOCE	GOCO	GRACE	ECCO	GECCO
R.M.S. [mm/s] \	DIR	TIM	SPW	DIR-2	TIM-2		CLS		
GOCE-DIR	**25**	12	11	10	12	11	12	28	27
GOCE-TIM	12	**23**	8	14	8	14	9	29	27
GOCE-SPW	11	8	**22**	14	8	14	9	28	27
GOCE-DIR-2	10	14	14	**28**	15	9	15	30	28
GOCE-TIM-2	12	8	8	15	**21**	14	7	28	27
GOCO01s	11	14	14	9	14	**28**	15	30	28
GRACE-CLS	12	9	9	15	7	15	**21**	27	26
ECCO	28	29	28	30	28	30	27	**34**	11
GECCO	27	27	27	28	27	28	26	11	**34**

5.5. Geodetic MDTs from GOCE-DIR-2, GOCO01s and ITG-GRACE2010s geoids

We intercompare here MDTs, which are based on one of the GOCE (GOCE-DIR-2), the GOCO01s and the ITG-GRACE2010s geoid. The differences in MDT are mapped in Figure 29. As with the intercomparison of the GOCE-MDTs there is no essential offset between the different 'geodetic' MDTs with maximum global mean difference of 2.8 mm, and all three correlations are again larger

than 0.99. The R.M.S. (which is essentially identical to the std.dev.) has values between 8 mm (GOCE-DIR-2 - GOCO01s) and 23 mm (GRACE-CLS - GOCE-DIR-2) comparable to those from the GOCE-MDT intercomparison.

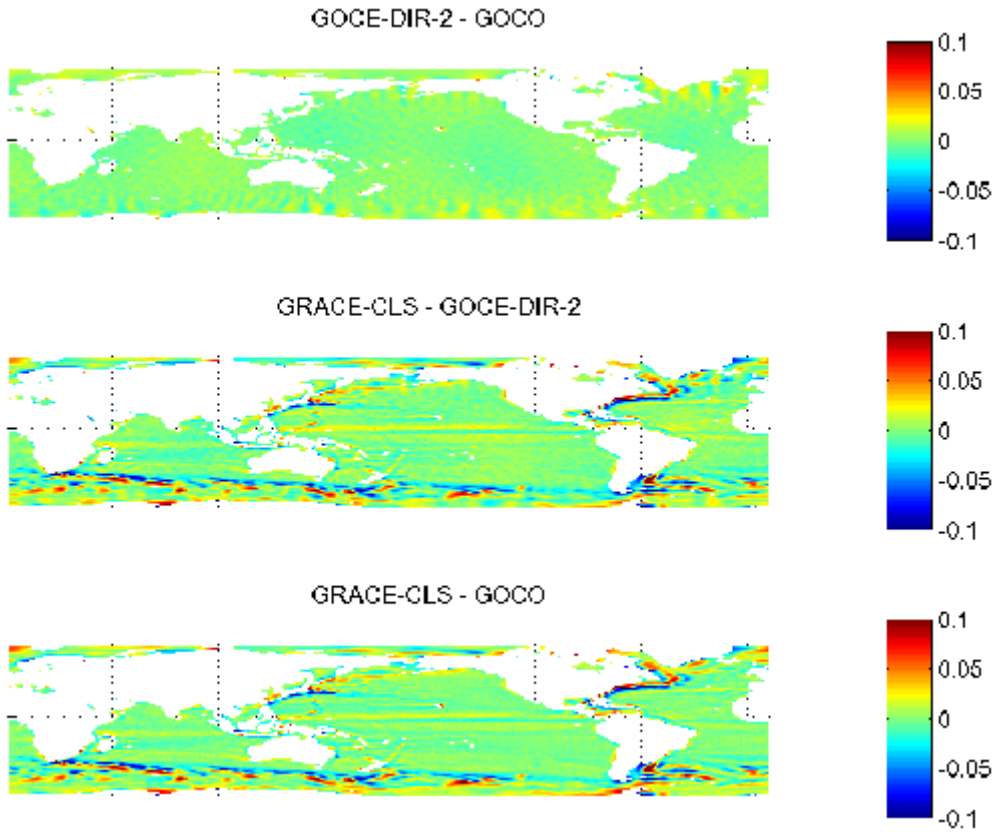

Figure 29: Differences in geodetic MDTs (m).

The spectral analysis (Figure 30) shows comparable discrepancies between the three MDT models for degrees 2-4. For all shorter length scales (< 5000 km) the GOCE-DIR-2 and GOCO MDTs closely agree with differences several times lower than the differences between each of the two maps and GRACE-CLS. The larger differences to GRACE-CLS are, however, below signal strength for all length scales.

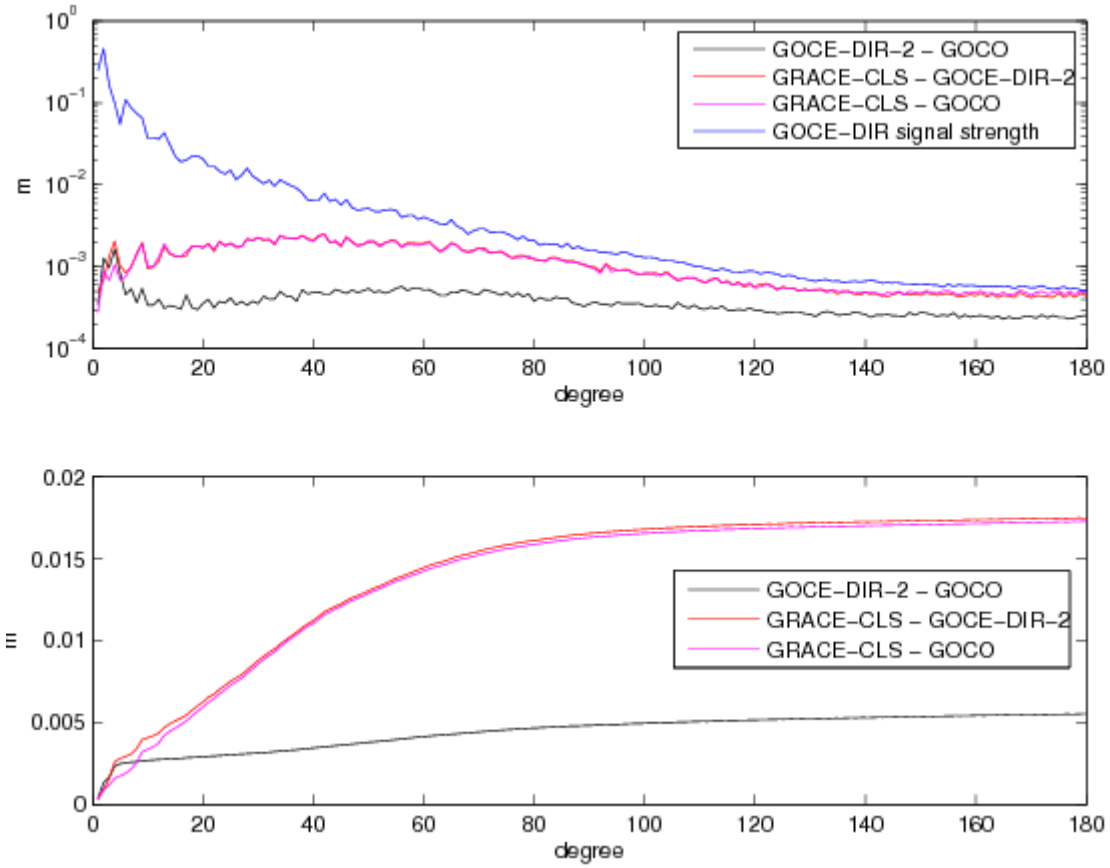

Figure 30: Spectral analysis of geodetic MDT differences. (top) Square root of degree variances (m); the signal strength of GOCE-DIR is added for comparison (see Fig. 2). (bottom) cumulated square root of degree variances.

The difference in geostrophic surface currents is displayed in Figure 31 and Figure 32 for the *U* and *V* component, respectively. As with the GOCE-MDTs the differences are on short latitudinal-scale zonal stripes with strongest values near the equator. Absolute global mean differences (see Tabs. 4 and 6) are 0.3 mm/s or lower for all comparisons and both directions. The differences in the *U* components are generally lower (R.M.S. between 6 mm/s and 17 mm/s) than in the *V* components (R.M.S. between 8 mm/s and 34 mm/s, see Tabs. 5 and 7), with close agreement of the GOCO and GOCE-DIR-2 maps and larger differences for comparisons with GRACE-CLS, for both directions. Correlations (Tabs. 4 and 6) are very high in all comparisons (between 0.97 and 1.00).

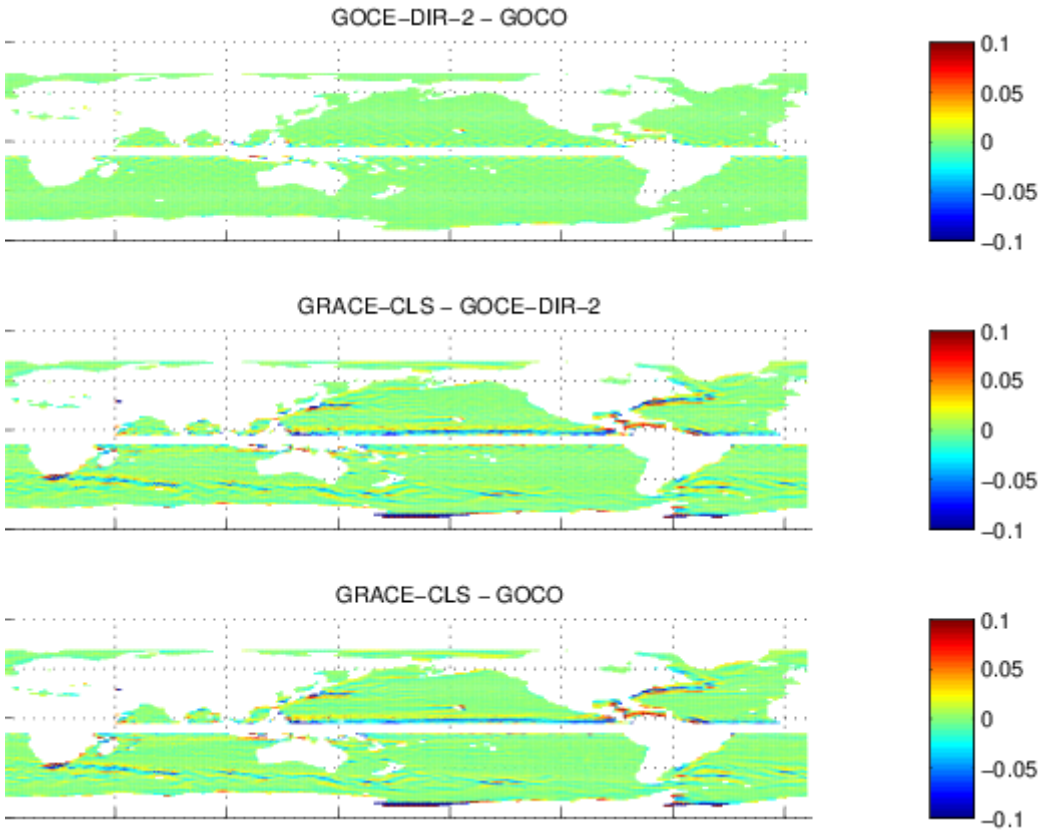

Figure 31: Differences in zonal geostrophic surface currents (m) for the geodetic MDTs.

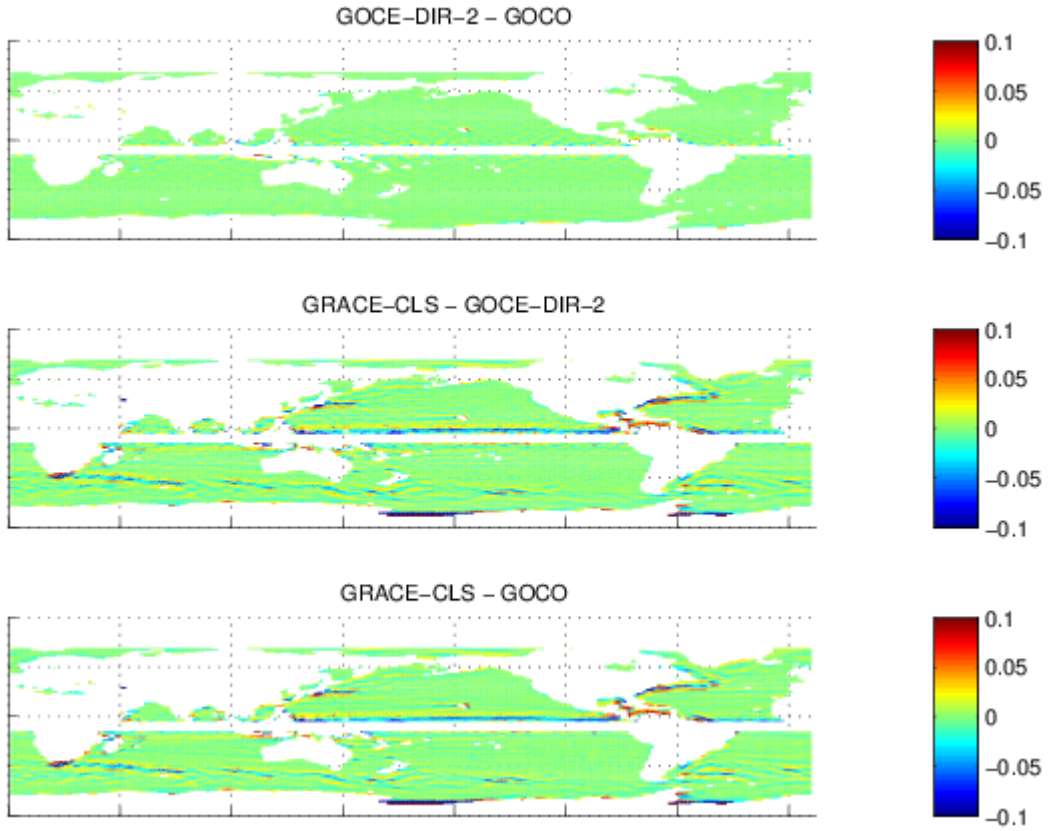

Figure 32: Differences in meridional geostrophic surface currents (m) for the geodetic MDTs.

5.6. Comparison to hydrodynamic models

All 'geodetic' MDTs we analyzed, when subtracted from the same MSS, closely agree, with R.M.S. values of never more than 25 mm (see Tab. 2). In comparison, the two MDTs from the hydrodynamic models show a larger disagreement among each other (68 mm) and even larger differences to the 'geodetic' MDTs (69 mm - 75 mm for ECCO, 86 mm -104 mm for GECCO). In Figure 33, Figure 34, Figure 35 we use the GOCE-DIR-2 solution as a representative for the 'geodetic' MDTs, which we compare with the modeled MDTs.

The differences between the MDTs is displayed in Figure 33. ECCO and GOCE-DIR-2 mainly disagree in regions of strong current systems, as the ACC, the Gulf Stream and the Kuroshio, and also along two zonal stripes near the equator. The two models disagree mainly in the structure and strength of the strong meridional MDT gradient in the Southern Ocean, with weaker gradients in GECCO. The difference between GOCE-DIR and GECCO is mainly added up by the differences between the two models and the discrepancy of ECCO compared to GOCE-DIR.

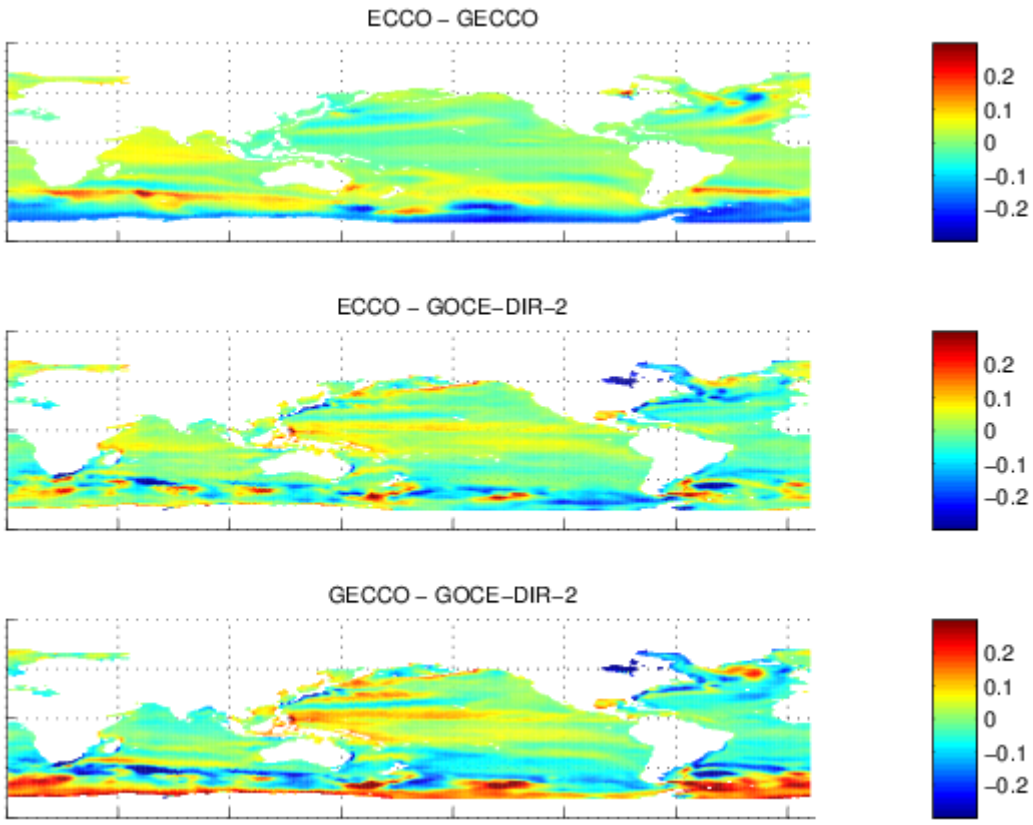

Figure 33: Differences in MDT (m) when comparing the geodetic GOCE-DIR with hydrodynamic model solutions.

From the spectral analysis (Figure 34) it emerges, that the models disagree mainly on the long spatial scales, and that for degrees >30 (≈700 km) the differences to GOCE-DIR-2 is almost identical for both models, while for longer scales, ECCO is closer to the 'geodetic' MDT than GECCO.

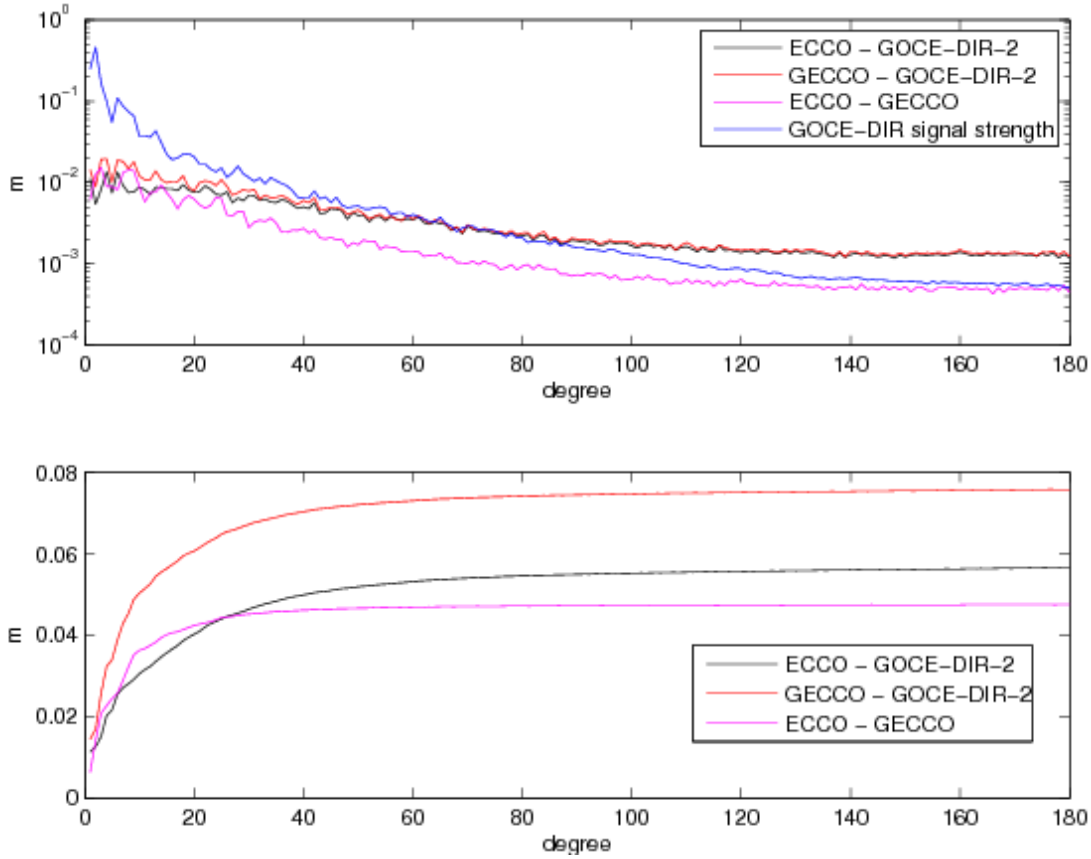

Figure 34: Spectral analysis of MDT differences comparing the geodetic GOCE-DIR with hydrodynamic model solutions. (top) Square root of degree variances (m); the signal strength of GOCE-DIR is added for comparison (see Fig. 2). (bottom) cumulated square root of degree variances.

The geostrophic surface currents from the hydrodynamic models have on global average magnitudes very close to the geodetic solutions for the U component (65 mm/s (GECCO) and 67 mm/s (ECCO), compared to values between 58 mm/s and 67 mm/s, see Tab. 5), while for the meridional direction current velocity is smaller (34 mm/s for both models compared to 43 mm/s - 82 mm/s for the geodetic solutions, see Tab. 7). The mapped velocity differences for the zonal component (Figure 35) repeat the zonal structure we found also in the geodetic solutions, but with larger overall differences when comparing any of the two models with the GOCE-DIR-2 solution (39 mm/s for GECCO, 43 mm/s for ECCO, compared to around 20 mm/s or less for intercomparison of geodetic solutions). The global mean difference between GECCO and ECCO is, however, only 18 mm/s. For the V component (see Figure 36), due to the generally weak currents in the hydrodynamic models, the discrepancy to GOCE-DIR-2 (29 mm/s for GECCO and 30 mm/s for ECCO, see Tab. 7) is comparable to the overall absolute velocities (34 mm/s for both models). As with the *U* component, the discrepancy between ECCO and GECCO is with 11 m/s much smaller than the difference to the geodetic solutions.

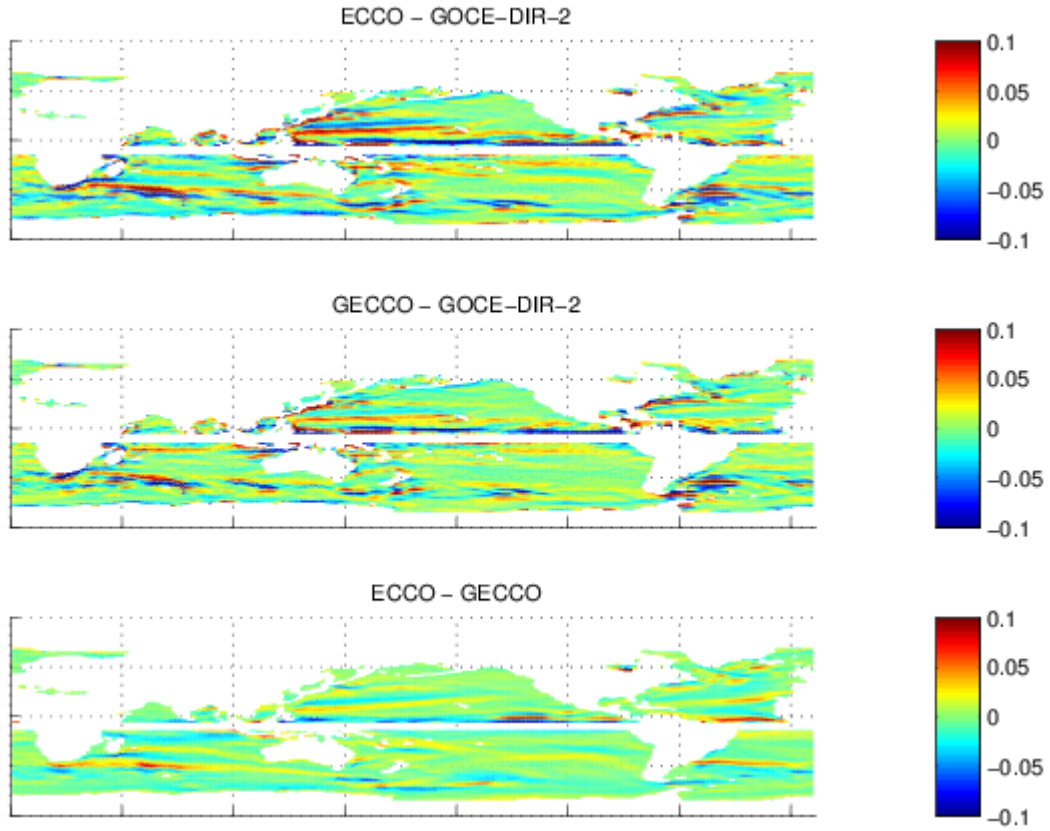

Figure 35: Differences in zonal geostrophic surface currents (m) when comparing the geodetic GOCE-DIR with hydrodynamic model solutions.

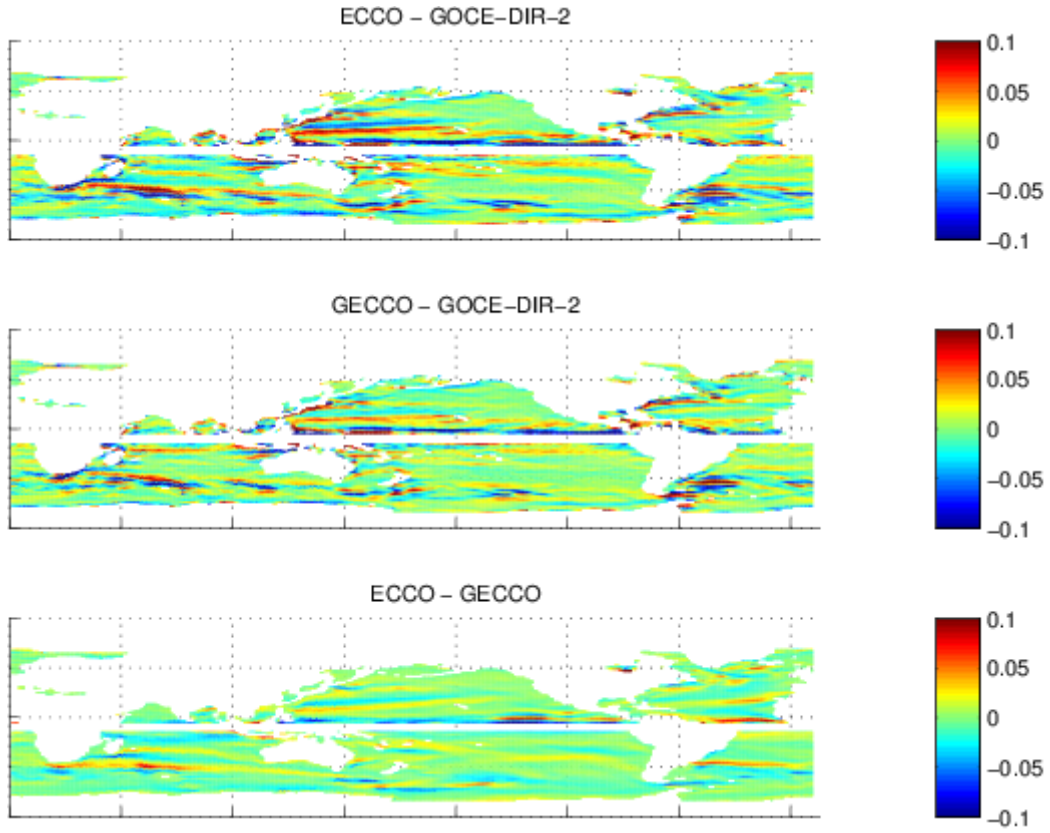

Figure 36: Differences in meridional geostrophic surface currents (m) when comparing the geodetic GOCE-DIR with hydrodynamic model solutions.

5.7. Summary

In this section, we have used the five GOCE geoids, a recent GRACE solution (ITG-GRACE2010s) and a GRACE/GOCE combined solution (GOCO01s) for intercomparison of geodetic MDTs and comparison with two integrations of hydrodynamic models (ECCO and GECCO). The five GOCE-MDTs agree fairly close to each other and the GOCO01s and GRACE solutions, if the same MSS is applied. Large differences are found, when 'geodetic' MDTs are compared to hydrodynamic models. While ECCO and GECCO disagree mainly on the large scale, especially in the Southern Ocean, the disagreement to the 'geodetic' solutions encompasses also shorter scales. While the MDT is found as a very robust signal, especially when regarding only geodetic MDTs and only one MSS, the geostrophic surface currents have a larger uncertainty, especially for the generally smaller meridional velocity component. Among the 'geodetic' solutions the differences in zonal velocities are in the order of one fourth of the overall velocity, and one half for the meridional component. When the hydrodynamic models are compared to the 'geodetic' solutions, the differences are, in an absolute sense, even larger for the *U* component, and about two third of the overall absolute velocities. For the *V* components, the differences are comparable to the (small) magnitude of the modeled meridional current velocities.

6. CONCLUSION

This report has described the validation work that has been carried out in the framework of the GUT2 WP4000 project to assess the accuracy of the preliminary GOCE geoid models delivered by HPF. The first two releases have been used, respectively based on two and six months of GOCE data.

Geodetic MDTs have been computed from the 5 different geoid models (2 models based on the direct approach, two models based on the time-wise approach, and one model based on the space wise approach) by subtracting each model from an altimetric Mean Sea Surface and further filtering the resulting field to get rid of the geoid omission errors and filter out the geoid and the MSS commission errors.

The accuracy of the obtained MDT has been assessed by comparing them to other MDT solutions:

- Geodetic MDT based on the ITG-GRACE2010s geoid model
- A MDT computed by Niiler et al, 2003 from a dataset of drifting buoy velocities
- A dataset of synthetic mean velocities computed from the combination of drifting buoy velocities and altimetric velocity anomalies
- MDTs issued from the ECCO and GECCO hydrodynamical models
- A MDT computed by Rio et al, 2007 for the Mediterranean Sea based on ocean modeling and drifting buoy velocities.

This work has allowed to highlight:

- The superiority of using only two months of GOCE data compared to GRACE data when computing satellite-only solutions
- The strong impact of using 3 more times more GOCE data in the second HPF release compared to the first HPF release
- The positive impact at scales ranging between 120 and 200 km of using GOCE data to improve combined geoid models (where short scales are resolved using information derived from altimetric MSS)
- The efficiency of the validation methods used to intercompare the different geoid solutions ans assess their quality and defaults.

On the other hand, this study has allowed to highlight the following limits:

- of the current preliminary geoid models: The difficulty to use GOCE data to estimate the ocean MDT in the Mediterranean Sea. This region may be used as a challenging objective for testing the future geoid models.

- of the current filtering techniques: in the future, some more sophisticated filtering should be tested, using the information from the GOCE covariance error matrix.

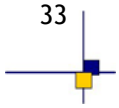

Annexe A - List of acronyms

TBC	To be confirmed
TBD	To be defined
AD	Applicable Document
RD	Reference Document